2011-01-01

Experimental And Numerical Investigation Of The Effect Of Fuel Composition On Flame Stability On A Gas Turbine Combustor

Gilberto Corona
University of Texas at El Paso, gcorona@miners.utep.edu

EXPERIMENTAL AND NUMERICAL INVESTIGATION OF THE EFFECT OF FUEL COMPOSITION ON FLAME STABILITY ON A GAS TURBINE COMBUSTOR

GILBERTO CORONA

Department of Mechanical Engineering

APPROVED:

Ahsan Choudhuri, Ph.D., Chair

Norman Love, Ph.D.

Vinod Kumar, Ph.D.

Stephen Stafford, Ph.D.

Benjamin C. Flores, Ph.D.
Acting Dean of the Graduate School

EXPERIMENTAL AND NUMERICAL INVESTIGATION OF THE EFFECT OF FUEL COMPOSITION ON FLAME STABILITY ON A GAS TURBINE COMBUSTOR

by

GILBERTO CORONA

THESIS

Presented to the Faculty of the Graduate School of

The University of Texas at El Paso

in Partial Fulfillment

of the Requirements

for the Degree of

MASTER OF SCIENCE

Department of Mechanical Engineering

THE UNIVERSITY OF TEXAS AT EL PASO

December 2011

Acknowledgements

This research was done with the support of the U.S. Department of Energy, under awards DE-FG26-08NT0001719 (Project Manager Norm Popkie). However, any opinions, findings, conclusions, or recommendations expressed herein are those of the authors and do not necessarily reflect the views of the Department of Energy.

Abstract

Gas turbines are used for power generation and aviation all over the world. Fossil fuels remain the main source of energy for the operation of gas turbines but the recent increase in environmental awareness has influenced government agencies to impose stringent limits on pollutant emissions from power generation plants. Pollutant emissions control is one of the major challenges for gas turbine designers. In this study, experimental methods and computational fluid dynamics (CFD) technologies are used to study the problems that arise when coal derived fuels are used in Gas Turbine Combustors.

Gas turbine designers need both experimental data and combustion models to design combustors that are efficient and have low emission characteristics. The trend in industry is towards less reliance in experimental methods and testing and more on numerical methods which would allow for shorter design cycles. The focus of this work is to obtain a comprehensive understanding of the instabilities that develop in gas turbine combustors and to map the operability range of a typical combustor for different fuel compositions. The modeling effort in this study will provide a critical insight on the flow-flame interaction through flow visualization techniques and the use of unsteady computational models. The outcomes from the research will provide design tools for developing gas turbine combustors fueled with gasified coal and other hydrogen containing fuels.

It is concluded in this study that when the hydrogen content of the fuel mixture is increased, for any given flow rate, the flashback propensity of the combustor increases. It was determined as well that syngas fuel derived from coals containing higher hydrogen content such as Brown and Bituminous are more prone to flashback than syngas derived from Lignite or Coke coal; this conclusion is congruent with the finding that hydrogen content increases the flashback propensity of a fuel mixture.

Table of Contents

List of Tables

List of Figures

1. Introduction

Gas turbines are used for power generation and aviation all over the world. Fossil fuels remain the main source of energy for the operation of gas turbines but the recent increase in the environmental awareness has influenced government agencies to impose stringent limits on pollutant emissions from power generation plants. Pollutant emissions control is one of the major challenges for gas turbine designers [1-5].

A fundamental understanding of combustion is of paramount necessity in order to design the next generation gas turbine combustors; the main focus with the operation of these advanced systems is to attain fuel flexibility and low emission characteristics. It is estimated that 90% of the world's energy demand is met by combustion processes. In the US 66% of the energy is derived from fossil fuels, 48% from coal alone [6]. Coal usage for power generation, however is responsible for over 40% of man-made CO_2 emissions [7] which is considered to play a major role in global warming.

It is estimated that the world's energy demands will rise by 60% by 2030, and fossil fuels will account for 85% of the total energy market [6]. The continued use of coal in the foreseeable future coupled with lower emission limits from regulatory agencies will require higher efficiencies in the design of the next generation gas turbine combustors and lower emission characteristics. To meet the energy demand using coal, the industry is going to have to rely on the combustion of gasified coal or syngas [2].

1.1 Swirl Stabilized Flames

Current design of Gas Turbine combustors uses swirling flows to stabilize the flame and lower the emissions by producing a more complete combustion. Swirling flows produce a central toroidal recirculation zone (CRTZ) (see Figure 1.1), which ensures efficient combustion conditions by allowing good fluid mixing and offering long residence time for complete reactions to take place[8-9].

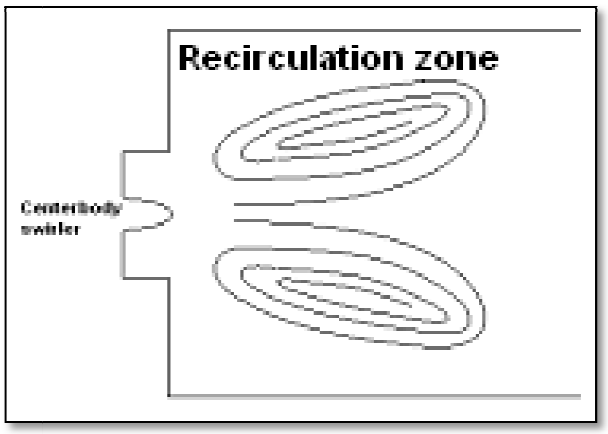

Figure 1.1 Central toroidal recirculation zone generated by the swirler

However, employing swirling flows has brought a number of concerns, especially flame flashback and flame blowout. Flame flashback is an inherent reliability problem in lean premixed combustion where the flame, instead of stabilizing completely within the combustion chamber, propagates upstream into the premixing zone against the gas stream. It involves coupled interactions of burning velocity, local flow-field quantities, and combustion instabilities [10-14]. Flashback is always unacceptable and must be avoided in all combustion conditions, since it increases pollutant emission and can also cause considerable damage to the hardware of the premixing zone and eventually to the entire combustion system. There are four mechanisms believed to be responsible to initiate flashback [11-12]:

- Flame propagation in the boundary layer,
- Turbulent flame propagation in the core flow,
- Violent combustion instabilities, and
- Combustion induced vortex breakdown (CIVB).

Additionally, the presence of hydrogen in syngas significantly increases the potential for flashback. Due to high laminar burning velocity and low lean flammability limit, hydrogen tends to shift the combustor operating conditions towards flashback regime. Even a small amount of hydrogen in a fuel blend triggers the onset of flashback by altering the kinetics and thermophysical characteristics of the mixture [10].

1.2 LEAN PREMIXED FLAMES

It is important at this point to make a distinction between two different combustions modes; premixed and non-premixed combustion. In premixed combustion the fuel and the oxidizer are mixed at the molecular level before entering the reaction zone. In non-premixed combustion the fuel and the oxidizer are kept separate until they enter the combustion zone so the reactants have to diffuse onto each other before they react forming a diffusion flame [15-16].

The formation of Nitric Oxides (NO_x) requires high energy when produced by the Zeldovich Mechanism which is the most common type for high temperature combustion. Thus the formation rate of NO_x has an exponential relationship with burning temperature [1, 15]. A measure taken to reduce NO_x formation is to reduce the residence time in the burner. However the opposite is true for the formation of CO. Lower temperatures and areas of incomplete combustion are associated with high rates of CO production [4]. Figure 1.2 shows the formation rate of CO and NO_x with respect to temperature.

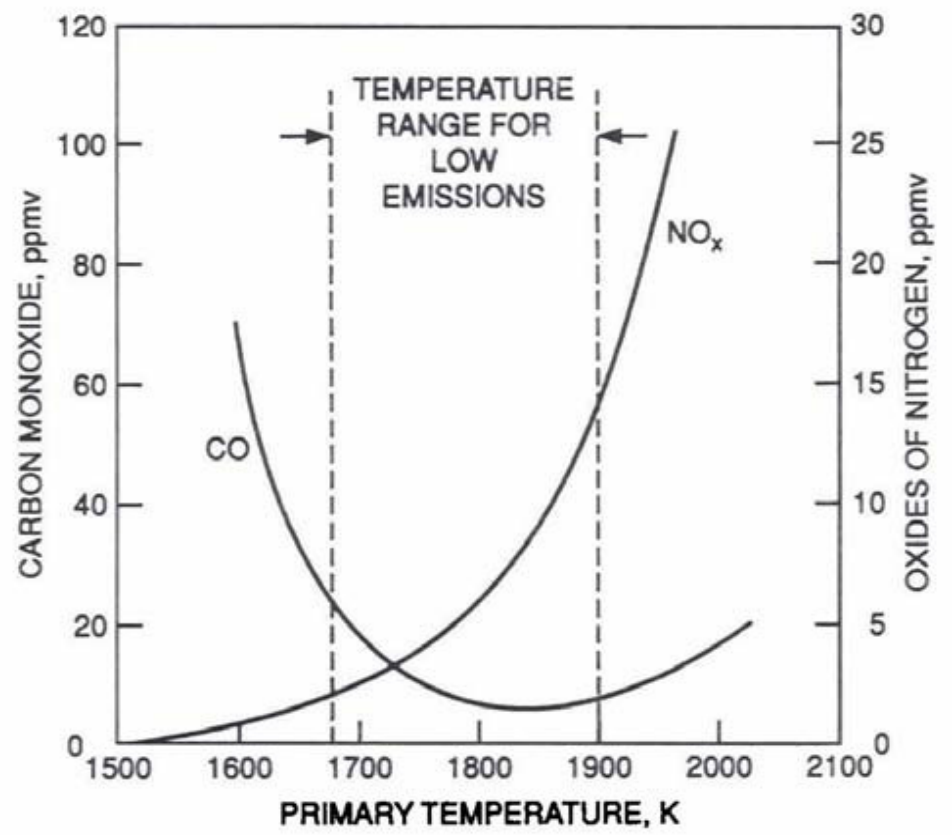

Figure 1.2 CO and NO_x formation relation to burning temperature [4]

It is evident from Figure 1.2 that in order to achieve low NO_x and CO emissions the reaction must take place at a narrow temperature band approximately between 1680 K and 1800 K. So for a gas turbine combustor to achieve low emission characteristics it has to be designed in such a way that it operates in this temperature range over the entire power output cycle.

As it can be seen in Figure 1.3, the burning temperature depends on the equivalence ratio (ϕ). Where ϕ is defined as the actual fuel-oxidant ratio (F/O) to the ratio $(F/O)_{st}$ for a stoichiometric process [15]. So if lower emissions are to be achieved, the mixture must burn either at a very lean however as stoichiometric conditions (ϕ=1) are approached NO_x pollutants tend to increase [16].

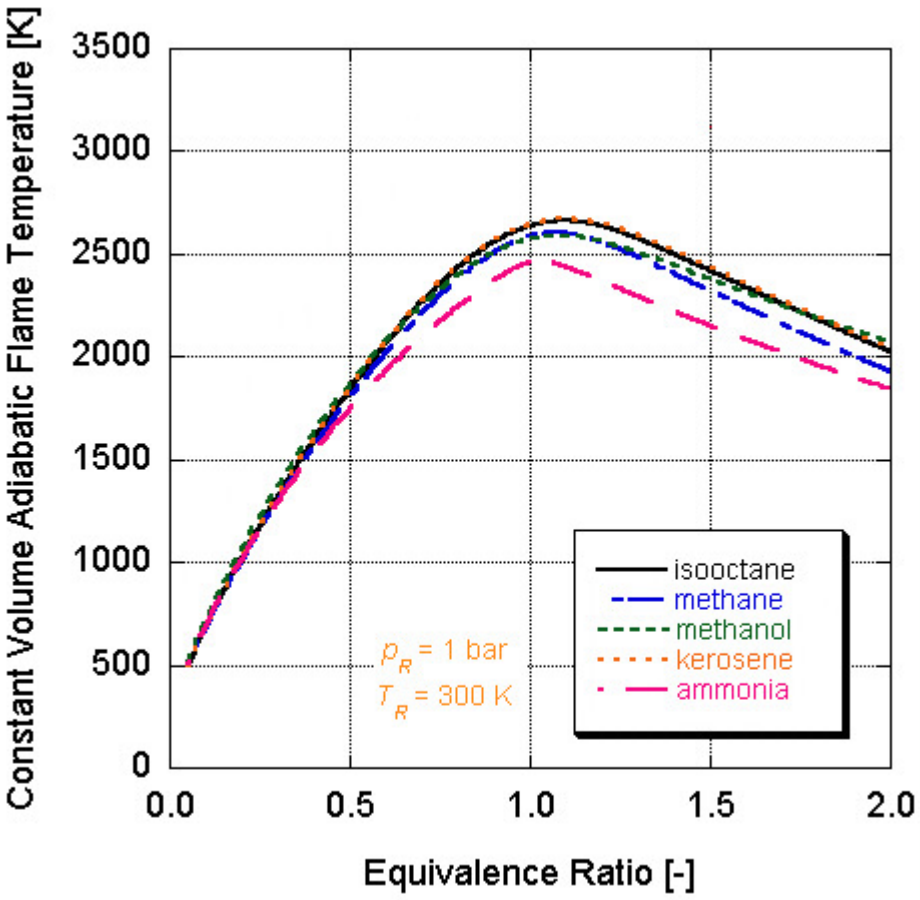

Figure 1.3 burning temperature vs Equivalence ratio (phi)

1.3 TURBULENCE MODELING

Accurate modeling of turbulent combustion is necessary for the development of future generation gas turbine combustors. The increase in computational power and recent advances in combustion models have made it possible for us to simulate complex flow configurations as well as time dependent problems that were unthinkable just a few years ago[5, 17-19].

Numerical simulations are cheaper to perform than experimental methods, thus they have grown in popularity in the last decades [18-19]. Key advantages of numerical simulations are the turnaround time, the overall monetary cost of the simulation and the possibility to probe for flow information over the entire domain, including data that otherwise would be very hard to measure in an experimental setup. However, accuracy is not guaranteed in numerical simulations, not under all conditions, especially combustion and transient phenomena, so results must be validated with experiments.

In most cases in engineering applications, especially those involving combustion, flows are found to be turbulent. This is in most cases desirable, since turbulence enhances the mixing process and heat transfer thus helping in the combustion process. Unfortunately turbulence does increase the complexity of the modeling effort.

A combustion model must treat in great detail the interaction of turbulence and chemical kinetics, as these two are highly coupled. These models must be less detailed than the combustion process occurring in the system because of the complexity of handling reaction mechanisms directly but with accurate treatment they can help us predict the behavior of specific combustion systems [17]. Thus they are of great importance for the design of combustion devices, which involve both scale and time dependent dynamic behaviors, characteristics that cannot be captured with time averaged models.

1.4 OBJECTIVES OF THE THESIS

The objective of this work is to obtain a comprehensive understanding of the instability that develops in gas turbine combustors when hydrogen containing fuels are used. Gas turbine designers need both experimental results and combustion models to design combustors that are efficient and have low emission characteristics. The trend in industry is towards less reliance in experimental methods and testing and more on numerical methods which would allow for shorter design cycles. This project's objectives are:

- Develop stability maps for the combustor in order to study the effects of fuel composition on flame flashback
- Use the PIV to develop a fundamental understanding of the flow-flame interaction inside the combustion chamber during stable operation of the combustor and in the onset of flashback
- Develop a computational model for the combustion chamber using the experimental data as basis for validation

2. Theory Review

2.1 GOVERNING EQUATIONS

2.1.1 Flow equations

The equations governing the flow of a chemically reacting gas mixture make use of mass, momentum, and energy conservation laws. In addition we have equations describing the conservation of chemical species, thermodynamic properties and reaction rates [1, 16]. We start with the mass, and momentum equations, also known as Navier-Stokes equations and species concentration:

Continuity

$$\frac{\partial \rho}{\partial t} + \frac{\partial(\rho u_k)}{\partial x_k} = 0 \tag{2.1}$$

Momentum

$$\frac{\partial \rho u_l}{\partial t} + \frac{\partial \rho u_k u_l}{\partial x_k} = -\frac{\partial p}{\partial x_l} + \frac{\partial \tau_{lk}}{\partial x_k} + \rho \sum_{i=1}^{N} Y_i f_{il} \tag{2.2}$$

where τ_{lk} is the viscous stress tensor

$$\tau_{lk} = \mu\left(\frac{\partial u_l}{\partial x_k} + \frac{\partial u_k}{\partial x_l} - \frac{2}{3}\frac{\partial u_m}{\partial x_m}\delta_{lk}\right) \tag{2.3}$$

Species conservation

$$\rho \frac{\partial Y_i}{\partial t} + \rho u_k \frac{\partial Y_i}{\partial x_k} = -\frac{\partial J_{ik}}{\partial x_k} + \dot{w}_i \tag{2.4}$$

Throughout this study Cartesian tensor notation will be used, where k, l, and m are indices that imply summation when repeated. The symbols x_k, u_k, ρ, p, Y_i, and J_{ik} represent, respectively, the coordinate direction k, velocity component in k, density, pressure, mass fraction of species i, and the molecular diffusion flux of species i in direction k. The term f_{il} represents body forces acting on species i in the direction l. Also, $\dot{w}_i$ is the rate of production or destruction of species i due to reactions. The molecular diffusion flux J_{ik} can be approximated by

$$J_{ik} = -\rho D_i \frac{\partial Y_i}{\partial x_k} \tag{2.5}$$

where D_i is a diffusion coefficient.

Solving for pressure in the equation of state we get

$$\boldsymbol{p = \rho RT \sum_{i=1}^{N} \frac{Y_i}{W_i}} \tag{2.6}$$

where R is the universal gas constant and W_i is the molecular weight of species *i*.

The enthalpy of the mixture is calculated with

$$\boldsymbol{h = \sum_{i=1}^{N} Y_i h_i} \tag{2.7}$$

where

$$\boldsymbol{h_i = h_i^0 + \int_{T^0}^{T} c_{p,i} dT} \tag{2.8}$$

Where h_i^0 is the standard specific heat of formation of species *i* at temperature T^0.

Writing the energy equation in terms of entropy we get

$$\boldsymbol{\rho \frac{\partial h}{\partial t} + \rho u_k \frac{\partial h}{\partial x_k} = \frac{\partial p}{\partial t} + u_k \frac{\partial p}{\partial x_k} + \tau_{lk} \frac{\partial u_l}{\partial u_k} - \frac{\partial q_k}{\partial x_k} - \rho \sum_{i=1}^{N} h_i f_{ik} \frac{\partial Y_i}{\partial x_k} + q_{rad}} \tag{2.9}$$

where q_k is the heat flux and can be expressed by:

$$\boldsymbol{q_k = -\lambda \frac{\partial T}{\partial x_k} - \rho \sum_{i=1}^{N} h_i D_i \frac{\partial Y_i}{\partial x_k}} \tag{2.10}$$

where λ stands for the thermal conductivity.

At this point it would be good introduce three dimensionless parameters used to characterize molecular transport. The first is the Prandtl number, which is the ratio of momentum diffusivity to thermal diffusivity. The second is the Schmidt number, which is the ratio of momentum diffusivity to mass diffusivity. And the third is the Lewis number defined as the ratio of thermal diffusivity to mass diffusivity:

$$\boldsymbol{Pr = \frac{\nu}{\alpha} = \frac{\mu c_p}{\lambda}} \tag{2.11}$$

$$\boldsymbol{Sc_i = \frac{\nu}{D_i} = \frac{\mu \rho}{D_i}} \tag{2.12}$$

$$\boldsymbol{Le = \frac{\alpha}{D_i} = \frac{Sc_i}{Pr}} \tag{2.13}$$

where

$$\boldsymbol{c_p = \sum_{i=1}^{N} Y_i c_{p,i}} \tag{2.14}$$

As it stands, equation (2.7) is too complex to use in a large scale simulation, but it can be greatly simplified if we make the following assumptions: (1) Compressibility effects are neglected. (2) Radiation is negligible. (3) Energy changes from body forces can be ignored. (4) The diffusion coefficient D_i for species i will be approximated by a common coefficient D for all species. (5) The Lewis number is unity so the Schmidt number of species i will be equal to the Prandalt number (Sc_i = Pr) [16]. The simplified entropy equation looks like this

$$\boldsymbol{\rho \frac{\partial h}{\partial t} + \rho u_k \frac{\partial h}{\partial x_k} = \frac{\partial}{\partial u_k}\left(\rho D \frac{\partial h}{\partial x_k}\right)} \tag{2.15}$$

2.1.2 Chemical Reaction Rate

The rate of production or destruction of species i ($\dot{w}_i$) that appears on equation (2.4) can be approximated by

$$\boldsymbol{\dot{w}_i = W_i \sum_{i=1}^{N} (\nu''_{ik} - \nu'_{ik}) \bar{w}_k} \tag{2.16}$$

Here the exponents $\boldsymbol{\nu'_{ir}}$ and $\boldsymbol{\nu''_{ir}}$ are the stoichiometric coefficients of species i in reaction r in the forward and backwards direction, respectively. These exponents are obtained from a reaction mechanism in the form

$$\boldsymbol{\sum_{i=1}^{N} \nu'_{ki} M_i \underset{k_{bk}}{\overset{k_{fk}}{\leftrightarrows}} \sum_{i=1}^{N} \nu''_{ki} M_i} \tag{2.17}$$

The term $\bar{w}_r$ in equation (2.13) represents the rate of reaction r and it is calculated from:

$$\boldsymbol{\bar{w}_k = k_{fk} \prod_{j=1}^{N} \left(\frac{\rho Y_j}{W_j}\right)^{\nu'_{jr}} - k_{bk} \prod_{j=1}^{N} \left(\frac{\rho Y_j}{W_j}\right)^{\nu''_{jr}}} \tag{2.18}$$

here k_{fk} and k_{bk} are the forward and backward reaction rate coefficients of reaction k, and can be expressed as

$$\boldsymbol{k_{fk} = A_{fk} T^{\alpha_{fk}} e^{\left(\frac{-E^a_{fk}}{RT}\right)}} \tag{2.19}$$

$$\boldsymbol{k_{bk} = A_{bk} T^{\alpha_{bk}} e^{\left(\frac{-E^a_{bk}}{RT}\right)}} \tag{2.20}$$

where A_{fk}, A_{bk}, α_{fk}, α_{bk}, E^{a}_{fk}, and E^{a}_{bk} are constants of the empirical nature contained in the reaction mechanism[1, 16].

2.2 MODELING TECHNIQUES

Two different models are needed in order to convert the governing equations into a closed set: a turbulence model for the Reynolds Stresses and a combustion model for the reaction rate term. And although these models are covered separately and have very little similarities, in reality they are highly coupled [16-19].

2.2.1 Modeling Turbulent Flow

The governing equations of fluid flow (Navier-Stokes equations) are perfectly deterministic, and in theory we could solve them numerically. In reality, however, this turns out to be quite difficult because the velocity behaves in such a chaotic manner that the computing power available today is not enough to solve for u for typical domain sizes and flow speeds [20-21]. The term responsible for this behavior of the velocity is the non-linearity term in the momentum equation (convection of momentum). However, even if the velocity behaves in a random manner, the statistical properties of the flow are quite reproducible. That is why most turbulence theories focus in the determination of the statistical properties of the flow and not the velocity [20-22].

Reynolds Averaged Navier Stokes Equations (RANS)

A classical approach, and the most basic one, was first derived by Reynolds. The approach involves the decomposition of the velocity term into its mean and the fluctuating term [21]

$$\boldsymbol{u(x,t) = \bar{u}(x) + u'(x,t)} \tag{2.21}$$

This is referred as the Reynolds decomposition. Substituting equation 2.22 into the governing equations, and taking the time average we end up with:

$$\boldsymbol{\frac{\partial(\bar{u}_k)}{\partial x_k} = 0} \tag{2.22}$$

$$\boldsymbol{\frac{\partial \rho \bar{u}_k \bar{u}_l}{\partial x_k} = -\frac{\partial \bar{p}}{\partial x_l} + \frac{\partial}{\partial x_k}\left[\bar{\tau}_{lk} - \rho \overline{u'_k u'_l}\right]} \tag{2.23}$$

When we take the time average all the time dependent terms disappear, including $u'(x,t)$. You can see that the averaged Navier Stokes equations are very similar to the regular Navier Stokes equations except for the extra term $\rho\overline{u_k' u_l'}$ in the momentum equation which arises because of the nonlinear convective term and is referred as the Reynolds Stress, even though is not a real stress.

However in combustion modeling it is usually more convenient to use a mass-weighted average or Favre averages [16, 20] defined as

$$\tilde{\boldsymbol{\varphi}} = \frac{\overline{\rho\varphi}}{\bar{\rho}} \tag{2.24}$$

The Favre decomposition is written as

$$\boldsymbol{\varphi}(\boldsymbol{x},\boldsymbol{t}) = \tilde{\boldsymbol{\varphi}}(\boldsymbol{x}) + \boldsymbol{\varphi}''(\boldsymbol{x},\boldsymbol{t}) \tag{2.25}$$

Where $\varphi''(x,t)$ is the fluctuating component. Applying a Favre average to the mass, momentum and species equations yield [20-21]:

$$\frac{\partial\bar{\rho}}{\partial t} + \frac{\partial(\bar{\rho}\tilde{u}_k)}{\partial x_k} = 0 \tag{2.26}$$

$$\frac{\partial\bar{\rho}\tilde{u}_l}{\partial t} + \frac{\partial\bar{\rho}\tilde{u}_k\tilde{u}_l}{\partial x_k} = -\frac{\partial\bar{\rho}\widetilde{u_l''u_k''}}{\partial x_k} - \frac{\partial\bar{p}}{\partial x_l} + \frac{\partial\bar{\tau}_{lk}}{\partial x_k} + \bar{\rho}\sum_{i=1}^{N}\widetilde{Y_i f_{il}} \tag{2.27}$$

$$\frac{\partial\bar{\rho}\tilde{Y}_i}{\partial t} + \frac{\partial\bar{\rho}\tilde{u}_k\tilde{Y}_i}{\partial x_k} = -\frac{\partial\bar{\rho}_i\widetilde{u_k''Y_i''}}{\partial x_k} - \frac{\partial\bar{J}_{ik}}{\partial x_k} + \bar{\dot{w}}_i \tag{2.28}$$

Both the Reynolds Averaged equations and the Favre averaged equations contain more unknowns than equations, therefore in order to solve for them a model for the terms $\rho\overline{u_k' u_l'}$ and $\bar{\rho}\widetilde{u_l''u_k''}$ must be provided. There are many models available for the Reynolds Stresses that vary in terms of rigor and modeling effort. Individual RANS models are not going to be covered in this thesis but some examples are: the k-ε model, k-ω, Spalart-Allmaras, LRR, Reynolds Stress Transport to name a few.

Large Eddy Simulation (LES)

In LES the large scales of the energy spectrum are resolved while the smaller scales are averaged and their effect is modeled using a Subgrid Scale (SGS) model [18]. The approach is justified in the

sense that larger structures within the flow contain higher levels of turbulent kinetic energy, do most of the transport, and are dictated by the geometry and boundary conditions as opposed to the smaller dissipating structures which are more isotropic and independent of the boundary conditions.

LES of turbulent combustion has gained a lot of attention in the academic community because it provides more detailed information of flow fields and reaction zones not possible with traditional Reynolds Averaged Navier-Stokes (RANS) models. The information obtained from an LES model is also important since it can provide information on flame behaviors not attainable through experimental means.

The governing equations for LES are obtained by applying a filtering operator Eq. (2.29) to the Navier-Stokes equations. The effect that this filtering operator has is that the scales smaller than the filter width are averaged out and their effect is modeled by means of a subgrid model. The filtering operator and the resulting incompressible governing equations for LES are presented in Eqns (2.29-2.33) [16, 21].

$$\overline{\emptyset}(\boldsymbol{x}) = \int_{\boldsymbol{D}} \emptyset(\boldsymbol{x}')\boldsymbol{G}(\boldsymbol{x},\boldsymbol{x}')\boldsymbol{dx}' \tag{2.29}$$

$$\frac{\boldsymbol{\partial\rho}}{\boldsymbol{\partial t}} + \frac{\boldsymbol{\partial}}{\boldsymbol{\partial x_i}}(\boldsymbol{\rho\bar{u}_i}) = \boldsymbol{0} \tag{2.30}$$

$$\frac{\boldsymbol{\partial}}{\boldsymbol{\partial t}}(\boldsymbol{\rho\bar{u}_i}) + \frac{\boldsymbol{\partial}}{\boldsymbol{\partial x_j}}\left(\boldsymbol{\rho\bar{u}_i\bar{u}_j}\right) = \frac{\boldsymbol{\partial}}{\boldsymbol{\partial x_j}}\left(\boldsymbol{\sigma_{ij}}\right) - \frac{\boldsymbol{\partial\bar{p}}}{\boldsymbol{\partial x_i}} - \frac{\boldsymbol{\partial\tau_{ij}}}{\boldsymbol{\partial x_j}} \tag{2.31}$$

Where

$$\boldsymbol{\sigma_{ij}} \equiv \left[\boldsymbol{\mu}\left(\frac{\boldsymbol{\partial\bar{u}_i}}{\boldsymbol{\partial x_j}} + \frac{\boldsymbol{\partial\bar{u}_j}}{\boldsymbol{\partial x_i}}\right)\right] - \frac{\boldsymbol{2}}{\boldsymbol{3}}\boldsymbol{\mu}\frac{\boldsymbol{\partial\bar{u}_k}}{\boldsymbol{\partial x_k}}\boldsymbol{\delta_{ij}} \tag{2.32}$$

And

$$\boldsymbol{\tau_{ij}} \equiv \boldsymbol{\rho\overline{u_i u_j}} - \boldsymbol{\rho\bar{u}_i\bar{u}_j} \tag{2.33}$$

It's important to note that the over bar operator ($\bar{}$) in the LES equations stands for a filtered quantity and not a time average like in the Reynolds Averaged equations. There are many subgrid-scale and filtering operators currently available. Based on initial simulation runs, selection of different models did not have significant effect in the results. Combustion model, however, is critical on the final solution

[17]. For this study the Smagorinsky-Lilly subgrid-scale model was used to compute the subgrid-scale stresses from Eqns (6-9).

$$\boldsymbol{\tau_{ij} - \frac{1}{3}\tau_{kk}\delta_{ij} = -2\mu_t\overline{S}_{ij}} \tag{2.34}$$

where

$$\boldsymbol{\overline{S}_{ij} \equiv \frac{1}{2}\left(\frac{\partial \overline{u}_i}{\partial x_j} + \frac{\partial \overline{u}_j}{\partial x_i}\right)} \tag{2.35}$$

In the Smagorinsky-Lilly model, the turbulent viscosity is modeled from

$$\boldsymbol{\mu_t = \rho L_s^2 |\overline{S}|} \tag{2.36}$$

where

$$\boldsymbol{|\overline{S}| \equiv \sqrt{2\overline{S}_{ij}\overline{S}_{ij}}} \tag{2.37}$$

L_s is computed using

$$\boldsymbol{L_s = min(\kappa d, C_s\Delta)} \tag{2.38}$$

2.2.2 Modeling Reacting Flow

In this study two combustion models are used and results from each compared. The first model uses species transport with eddy dissipation concept for treating the turbulence-chemistry interaction with detailed chemical mechanisms. Complete reaction mechanisms required extensive computational power and single step mechanisms could not accurately predict combustor temperatures and emission characteristics. Thus a reduced mechanism with a limited number of species and reaction steps was used with the model [19]. The software used for this combustion model is FLUENT which was coupled with CHEMKIN. FLUENT uses a convection-diffusion Eq. (2.39) to solve for the conservation of chemical species were the net rate of production of chemical species *i* (R_i) is modeled by Eq. (2.40)

$$\boldsymbol{\frac{\partial}{\partial t}(\rho Y_i) + \nabla \cdot (\rho \vec{u} Y_i) = -\nabla \cdot \vec{J}_i + R_i + S_i} \tag{2.39}$$

$$\boldsymbol{R_i = \frac{\rho(\xi^*)^2}{\tau^*[1-(\xi^*)^3]}(Y_i^* - Y_i)} \tag{2.40}$$

Where

$$\xi^* = C_\xi \left(\frac{\nu\varepsilon}{k^2}\right)^{1/4} \tag{2.41}$$

And

$$\tau^* = C_\tau \left(\frac{\nu}{\varepsilon}\right)^{1/2} \tag{2.42}$$

The mass diffusion is modeled by

$$\vec{J}_i = -\left(\rho D_{i,m} + \frac{\mu_t}{Sc_t}\right)\nabla Y_i - D_{T,i}\frac{\nabla T}{T} \tag{2.43}$$

3. Experimental Setup and Procedure

For this study a laboratory scale gas turbine combustor was used in order to study the effects of fuel composition on flame flashback as well as to analyze the flow-field/flame interaction dynamics at the moment of flashback. The combustor rig has three configurable modules: (i) inlet manifold with static mixture, (ii) swirl burner with mixing tube, and (iii) optically accessible combustion chamber. Figure 3.1 shows a schematic diagram of the gas turbine combustor.

The combustion chamber integrates a pilot flame with a mixture of methane and air. The swirl burner module is fitted with a quartz mixing tube. The quartz glass tube is needed for the high speed imaging of flashback inside the premixer. The fuel and air enter the inlet manifold through five alternate injection holes. The fuel-air mixture then passes through the static mixture section to eliminate any injection induced flow irregularities and to ensure proper mixing of air and fuel. The burner module can accommodate both centerbody and hubless swirlers. For the present study, experiments were carried out using centerbody swirlers only. As part of the experiments, a circular sleeve, as shown in figure 2.1, was fitted inside the inlet of the combustion chamber; this allows the air-fuel mixture to enter the combustion chamber through the passage between the sleeve and the centerbody of the swirler without experiencing any pressure drops due to the divergence at the inlet of the combustion chamber.

3.1 GAS TURBINE COMBUSTOR

3.1.1 Combustion Chamber

The combustion chamber is constructed in a rectangular-type cross-section whose side-walls are made up of quartz glass to provide optical access to the measuring instrumentation. The chamber is also fitted with a solenoid controlled exhaust port and emergency pressure relief systems for safety purposes. The entire combustor rig is positioned horizontally and can be operated at a maximum pressure of 624 kPa and it has a maximum power rating of 25 kW.

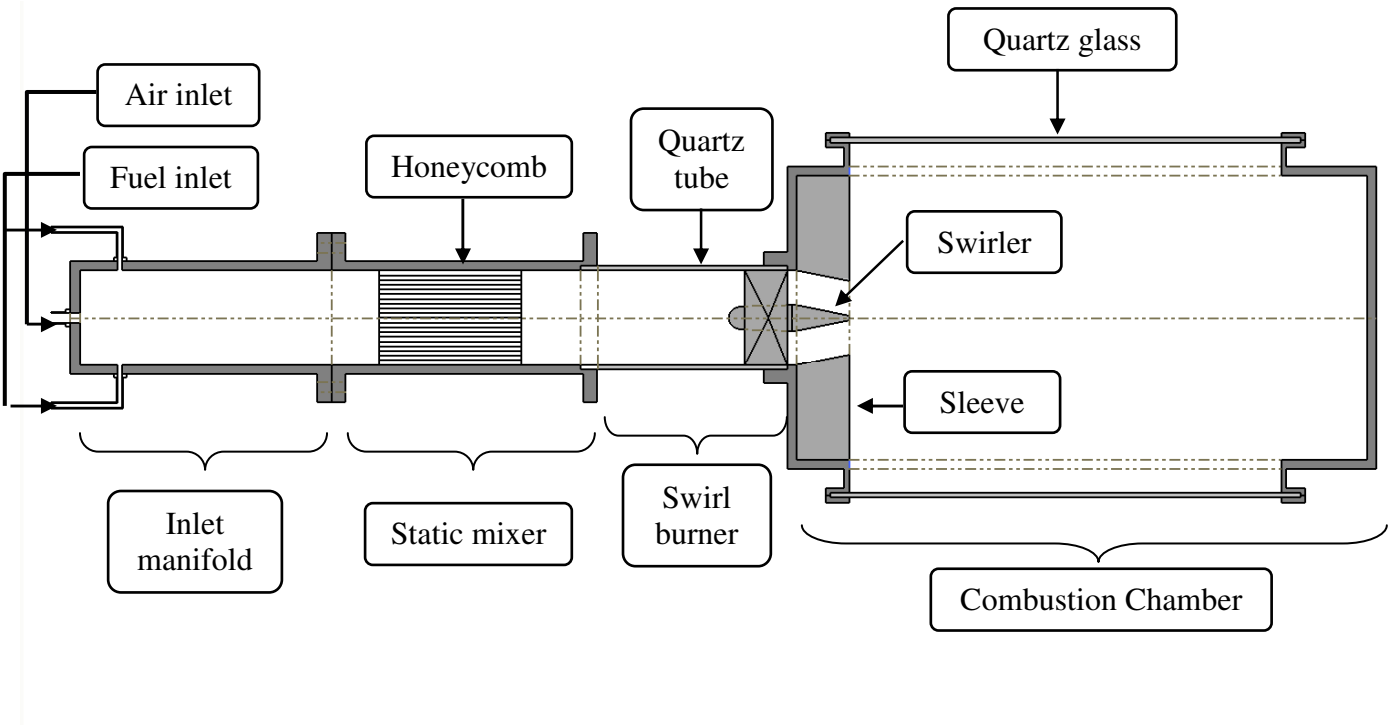

Figure 3.1 Schematic diagram of the gas turbine combustor

3.2.1 Swirler

Current design of gas turbine combustors makes use of swirl stabilized flames to achieve low emission characteristics. Swirling flows produce a central toroidal recirculation zone (CTRZ), which ensures efficient combustion conditions by allowing good fluid mixing and offering long residence time for complete reactions to take place [8-9].

For this study a centerbody swirler with 12 vanes and a swirl number of 0.97 was used, see figures 3.2 and 3.3. The swirl number is defined as the axial flux of swirl momentum divided by the

axial flux of axial momentum, times the equivalent nozzle radius. The swirl number can be related to the angle of a swirl vane and the geometry of the hub by [8]:

$$S = \frac{2}{3}\left[\frac{1-\left(\frac{d_h}{d}\right)^3}{1-\left(\frac{d_h}{d}\right)^2}\right]\tan\emptyset \tag{3.1}$$

Where d and d_h are nozzle and vane pack hub diameters, respectively. Plug flow axial velocity in the annular region is assumed. The centerbody of the swirler is made out of stainless steel while the body is made of aluminum which was anodized for higher temperature resistance. A sketch of the swirler with dimensions can be seen on figure 3.2. Figure 3.3 shows a picture of the swirler.

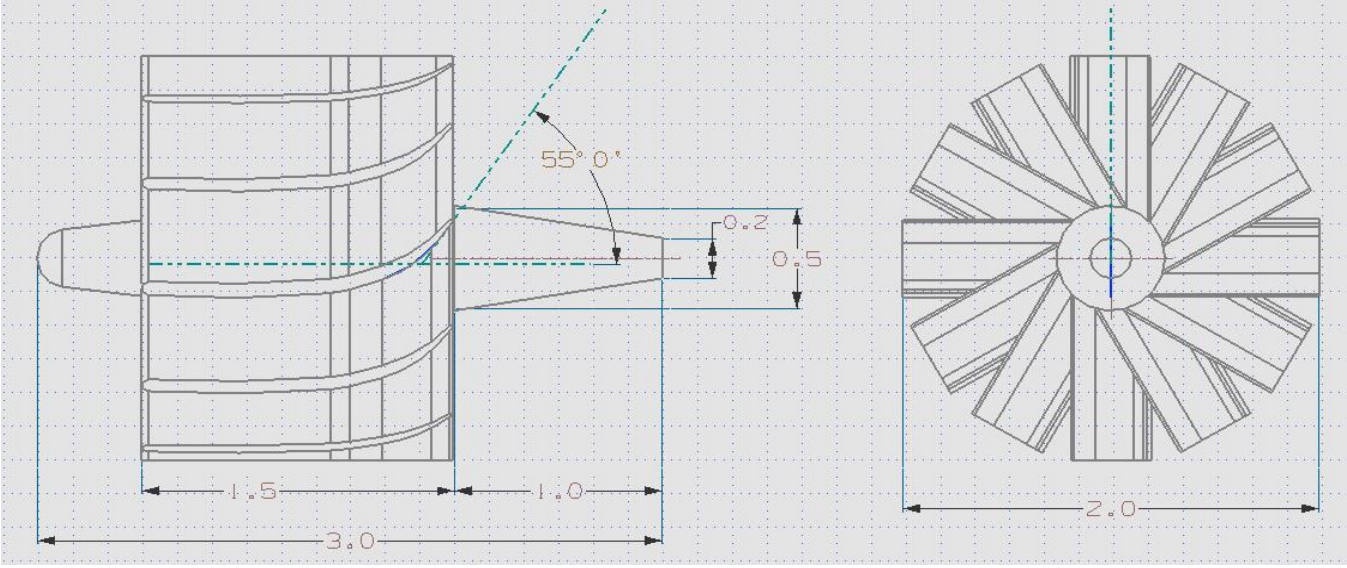

Figure 3.2 Sketch of the swirler

Figure 3.3 Centerbody swirler

3.2 FLOW MEASUREMENT DEVICES

Air was supplied to the rig through a high pressure rotary screw type compressor. All the gases (H_2, CO, CO_2, N_2, and Air) are stored separately in gas cylinders under 1600 psi pressure. The purity of these gases is 99%. Different flow meters are used in this experiment to control the volumetric flow rate which ranges from 0 to 500 LPM. Manual precision metering valves in conjunction with low-torque-quarter-turn plug valves are used to control and meter fuel and air flow rates. Prior to each experiment mass flow meters are calibrated using a laser based mass flow meter calibrator

3.2.1 Flow Meters

Digital mass flow meters Omega FMA 1700/1800 series (see figure 3.4) were used to measure the mass flow rate of air and fuel. The mass flow meters can work with temperatures ranging from 0^0C to 50^0C, handle pressures of up to 500 psig, a relative humidity of 70%, and they have an accuracy of ±1.5% of the full scale. The mass flow meters used in the present study varied from 0-10L/min to 0-500L/min. Prior to each experiment the flow meters were calibrated by using a Dry Cal Meter Calibrates also shown in Figure 3.4.

(a)

(b)

Figure 3.4 (a) Digital mass flow meters, (b) Dry Cal Meter Calibrates

3.2.2 Metering and Shutoff Valves

Manual precision metering valves (SS-SS4VH in figure 3.5) in conjunction with low-torque-quarter-turn plug valves were used to control and meter fuel and air flow rates. The Shutoff values (SS-4P4T4 in figure 3.5) were used to shut off the fuel flow from the pressurized gas cylinders.

(a) (b)

Figure 3.5 (a) Swagelok SS-SS4 VH Metering value 1, (b) Swagelok SS-SS4 VH Metering value 1

3.3 FLOW CHARACTERIZATION

Particle Image Velocimetry (PIV) is an optical method of flow visualization which is used to measure the instantaneous velocity components of a flow field. With the use state of the art systems we can achieve high resolutions in time and space allowing us to track individual structures within the flow. PIV is usually applied to non-reacting flows, but can also be used on reacting flows.

PIV is a non-intrusive method which allows us to calculate several flow field properties such as velocity, vorticity, turbulent intensity, and turbulent kinetic energy to name a few. In PIV the fluid is seeded with particles which ideally follow the flow faithfully. The fluid is then illuminated with the use of a laser sheet causing the particles to scatter light to the camera. PIV analysis requires two frames to be captured in order to compare them and produce a flow field. CCD cameras can capture two frames at very high speeds with only a few ns between frames. A post-processing software then calculates the displacement of the particles and the corresponding flow properties.

The system used for this study consists of a Phantom v310 camera, with a resolution of 1280 x 800 at 3250 fps and a maximum repetition rate of 500,000 fps (see Figure 3.6) and a high speed Nd:YLF LDY300 series laser with a maximum firing rate of 20 kHz and maximum energy output of 15 mJ per laser head operating at 1 kHz (see Figure 3.6). All the equipment was synchronized with Dantec Dynamics software.

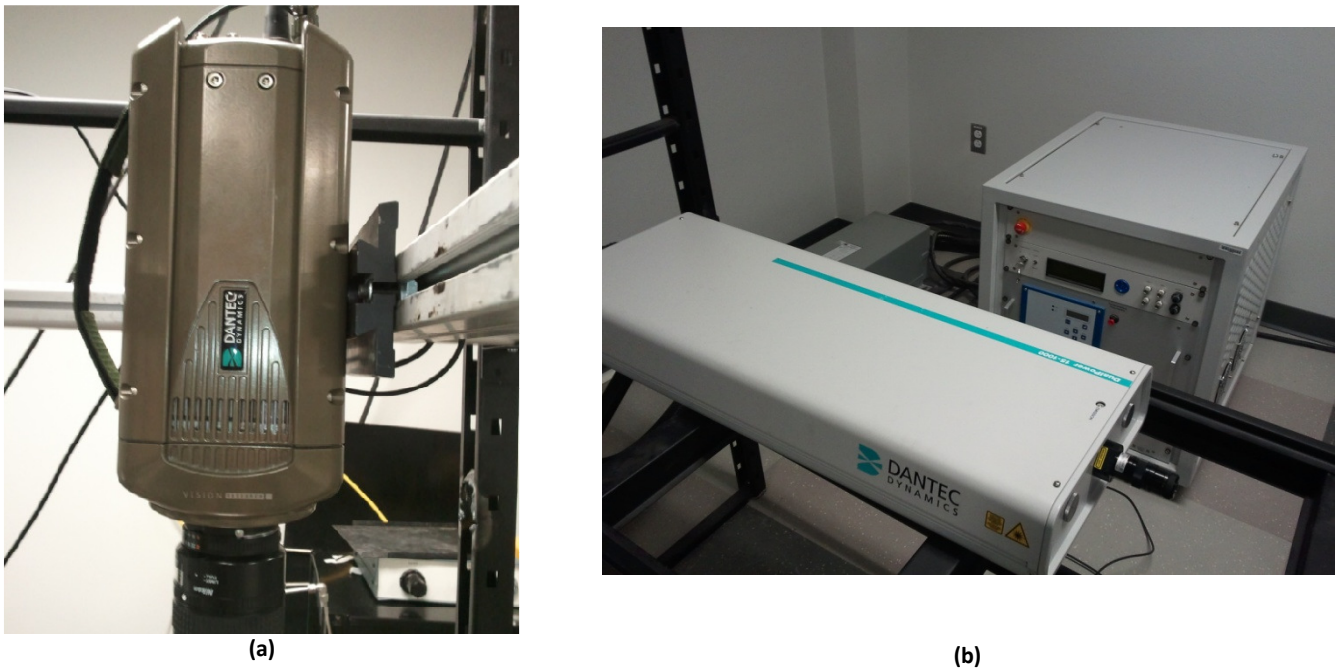

(a) (b)

Figure 3.6 (a) Phantom v310 camera, (b) LDY300 series high speed laser

A PS-10 Seeder system from SCITEK Consultants Ltd. was used to introduce the particles in the flow, see Figure 3.7. The seeder has a maximum working back pressure of 10 bar and can operate with temperatures in the range of 0 to 60°C. The PIV was used to characterize the flowfield in the combustion chamber operating at stable conditions and to analyze the changes in the flow when the flashback is initiated in order to identify the mechanisms responsible for this phenomenon. Figure 3.8 shows a picture of the entire setup. A schematic diagram of the setup can be seen on Figure 3.9.

Figure 3.7 PS-10 Seeder system from SCITEK

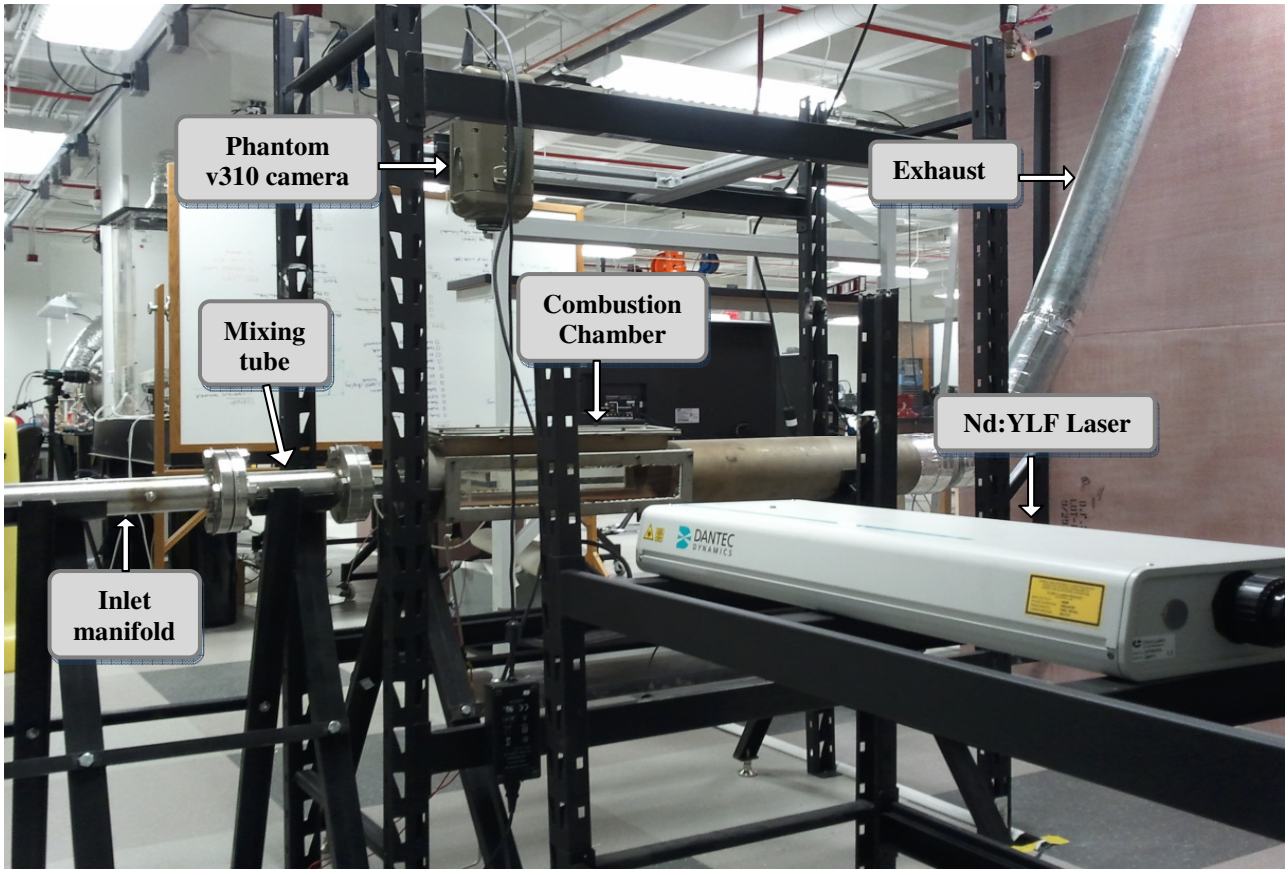

Figure 3.8 Gas turbine combustor setup with mounted high speed PIV

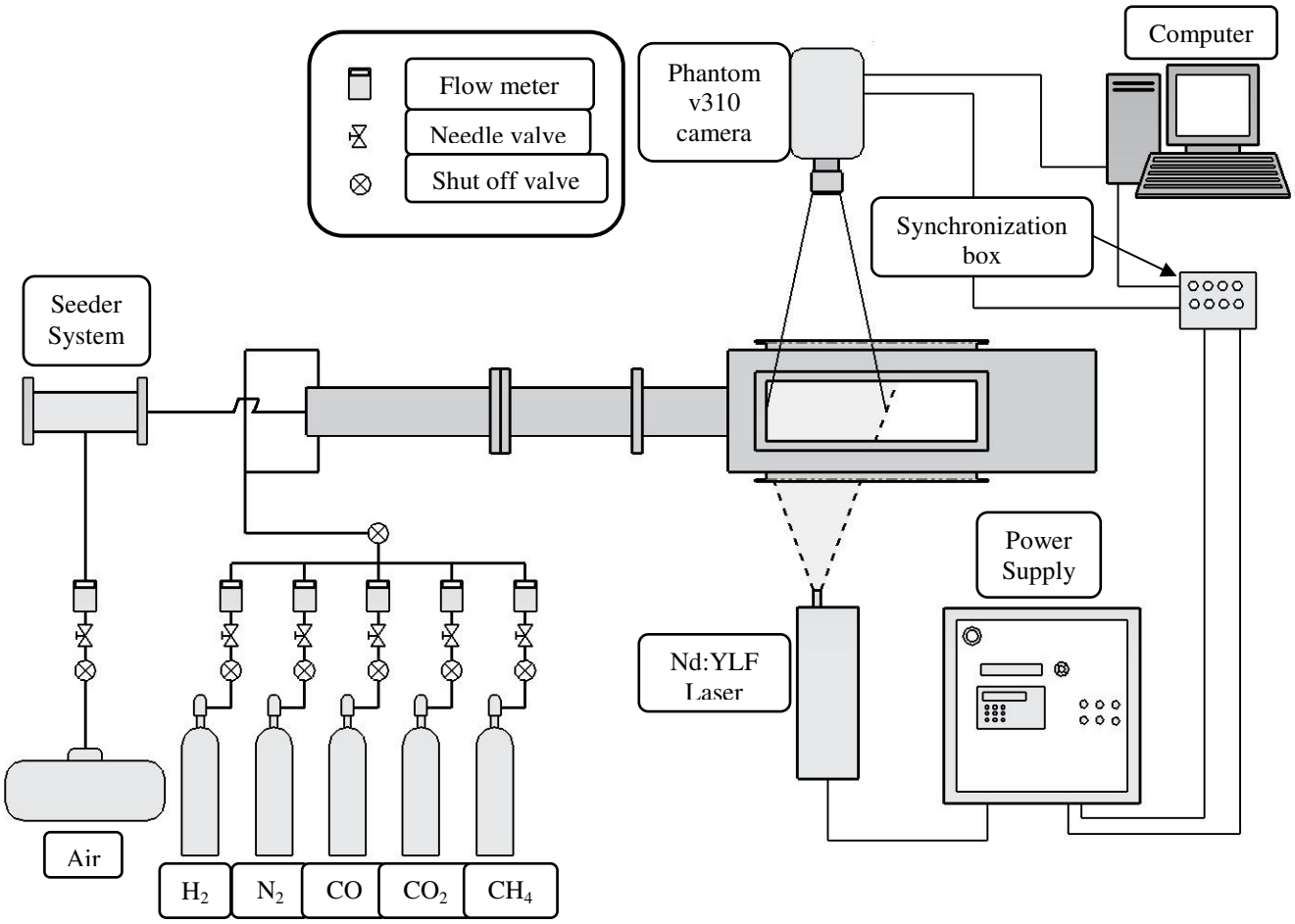

Figure 3.9 Schematic diagram of the setup

3.4 DESCRIPTION OF THE TEST MATRIX

The experiments performed with this setup have the following objectives:

1. Develop stability maps for the combustor in order to study the effects of fuel composition on flame flashback.
2. Use the PIV to develop a fundamental understanding of the flow/flame interaction inside the combustion chamber during stable operation of the combustor and in the onset of flashback.
3. Provide for validation cases for the combustion models developed in this thesis

This study focuses on the flame stability and behavior of gas turbine combustors using gasified coal or syngas fuel. The primary components of syngas are H2, CO2, CO, N2 and CH4, the exact

concentration of each component varies depending on the type of coal used. Table 3.1 shows syngas compositions from different types of coal.

For the first objective, systematic experimentations were performed on the combustion chamber using H_2-CO mixtures (primary constituents of syngas), methane and typical syngas compositions. Table 3.2 describes the test matrices used in this study to determine the flashback limits of the combustor with various fuel compositions. The stability maps for H_2-CO mixtures, Methane, and syngas fuels are presented in Chapter 4. The results of the PIV experiments are analyzed in Chapter 4, and again they are used in Chapter 5 to validate the numerical models developed in this thesis.

Table 3.1 Syngas composition from different coal sources

Gasification	Types of coal	CO (%)	H_2 (%)	CH_4 (%)	N_2 (%)	CO_2 (%)	Calorific Value (MJ/m^3)
Coal	Brown Coal	16	25	5	40	14	6.28
	Bituminous	17.2	24.8	4.1	42.7	11	6.13
	Lignite	22	12	1	55	10	4.13
	Coke	29	15	3	50	3	6.08
Wood		2.1	21	1.83	43	12	7.07

Table 3.2 test matix used in this study

Fuel	Fuel compositions tested	Volumetric flow rate range (LPM)	Range of bulk velocity in the premixer (m/s)
H_2 – CO	10% H_2 - 90% CO	138 ⟶ 315	1.4 ⟶ 3.2
	15% H_2 - 85% CO	144 ⟶ 272	1.4 ⟶ 2.7
	20% H_2 - 80% CO	112 ⟶ 261	1.1 ⟶ 2.5
CH_4	100% CH_4	20 ⟶ 389	1 ⟶ 3.5
Brown coal	100% Brown coal	69 ⟶ 232	0.56 ⟶ 1.9
Bituminous coal	100% Bituminous coal	121 ⟶ 274	1 ⟶ 2.25
Lignite	100% Lignite	48 ⟶ 148	0.4 ⟶ 1.2
Coke	100% Coke	79 ⟶ 201	0.65 ⟶ 1.65

4. Experimental Results and Discussion

Experimental measurements of the swirl stabilized flame were performed for a wide range of mixture compositions, equivalence ratios, and air mass flow. Initially, an experiment was carried out with Methane (CH_4)-air mixture and the result of that was used as the baseline for the rest of the experiments conducted in the present investigation. In the next stage, the investigation was focused on the effects of the fuel on CIVB flashback for various H_2-CO mixtures and actual syngas compositions.

To attain a flashback condition, the flow rates of fuel and air at the beginning were adjusted in such a way that the flame was stabilized completely inside the combustion chamber. The air flow rate was then decreased while maintaining the same fuel flow rate. Thus, the fuel-air mixture got richer and richer, and at a critical condition the flame propagated upstream and stabilized inside the burner tube. The flow rates of fuel and air at that condition were recorded for mapping purposes.

To investigate the corresponding reacting flow fields, the PIV system was simultaneously used. The analysis of the flow field in both stable and flashback conditions helped identify the mechanism that caused a stable flame to undergo flashback. The images obtained from PIV measurements provide the instantaneous velocity information with high spatial resolution over a period of time. In the present investigation the Proper Orthogonal Decomposition (POD) technique was used to post-process the data yielded by the PIV. Since its first introduction in analysis of flows around thirty years ago, POD has been recognized as a powerful tool for examining the fundamental mechanisms in flows by identifying the key dominant or coherent features. POD identifies the structures that contribute most to the energy of the flow and thus, enables the used to filter the lower energy modes, yielding a cleaner flow field, easier to analyze.

The use of POD has resulted in better flow-visualization images. For example, the first two images in Figure 4.1 represent the reaction flow field for CH_4-air mixture flame at stable condition at a particular equivalence ratio, frame 3(a) presents the vector flow field without POD and frame 3(b) represents the same condition but with the use of POD.

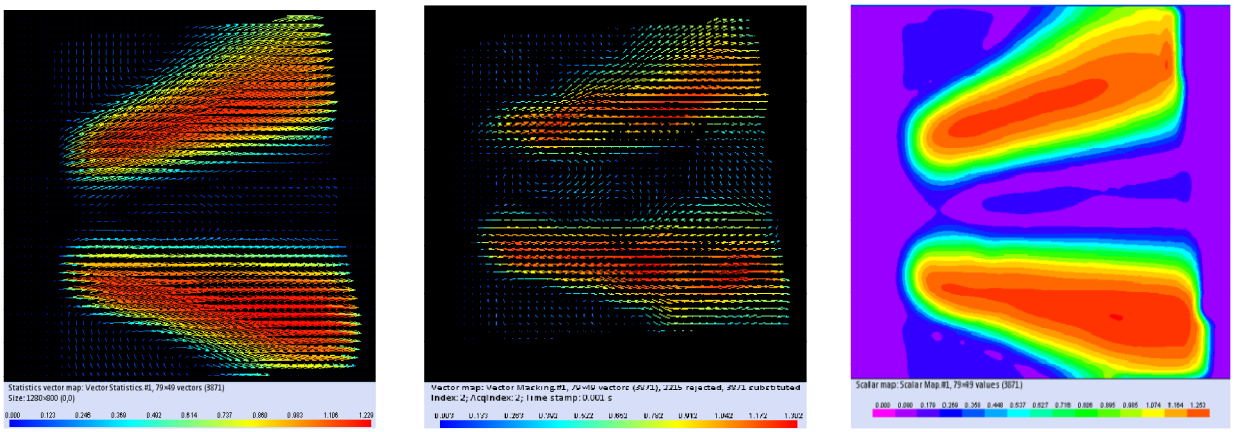

Figure 4.1 Reacting flow field for Methane-air operating in stable condition (a) vector image without POD, (b) vector image with POD, and (c) scalar map with POD

A comparison of these two images reveals that frame (b) shows the formation of recirculation zones enclosed by two high-velocity flame regions (residing close to the combustion chamber wall) more prominently than those seen in frame (a). The corresponding recirculation and high-velocity flame zones are even more noticeable in frame (c), which represents the scalar flow field of the same. Therefore, the flow visualization images from now on will be presented in the form of scalar maps.

4.1 VISUAL IDENTIFICATION OF CIVB FLASHBACK

The images shown in Figure 4.2 represent a series of sample photographs (acquired by the digital imaging system) showing how a flame, starting from a stable state (frame a), experiences flashback (frame d) due to CIVB; the upper row shows the photographic sequence of the phenomenon whereas the lower row represents the approximate and simple line diagram of the same. As seen in frame (a), initially the flame is stabilized in front of the swirler. It moves slowly upstream of the centerbody and starts oscillating with an increase in the equivalence ratio. The frequency of oscillation increases at higher equivalence ratios. This can be seen in frames (b) and (c), where the centerbody tip is more visible than that in frame (a). The flame stabilizes upstream of the centerbody with further increase in the equivalence ratio, see frame (d). This state of the flame is identified as the flashback situation; here the centerbody is much more prominent than that in all the previous frames.

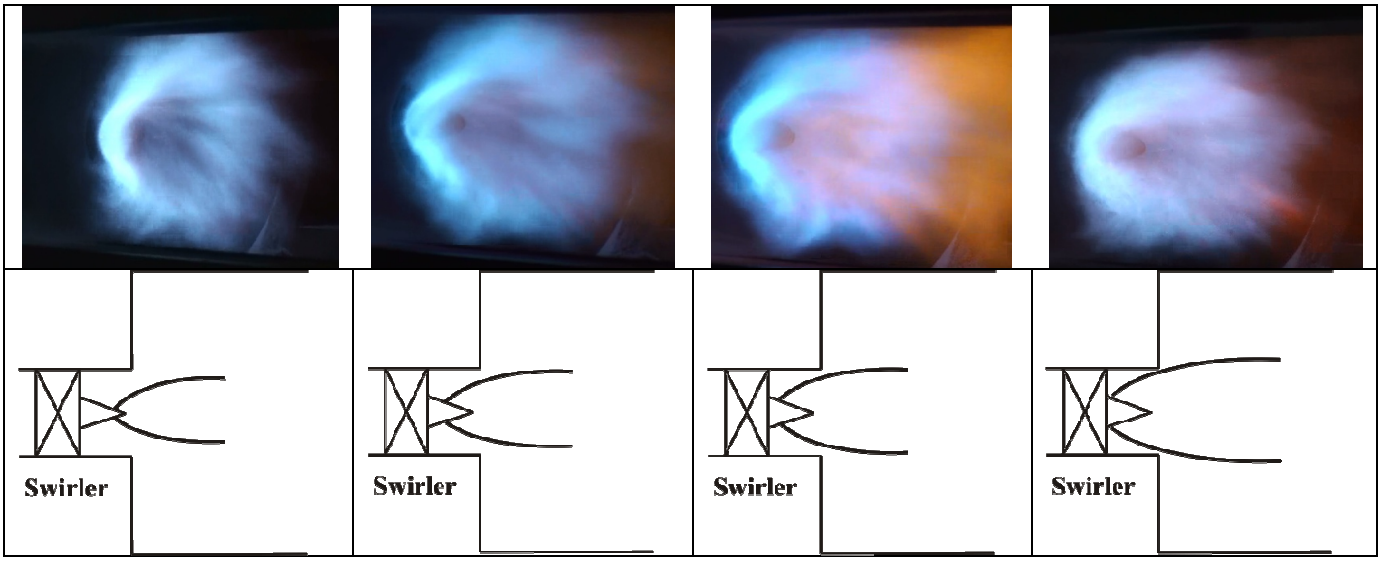

Figure 4.2 Sequence of a typical flashback phenomenon caused by CIVB with the upper row representing the photographic sequence and the lower row representing the same but by approximate lines only (not in scale).

4.2 BASELINE EXPERIMENTS WITH CH_4-AIR MIXTURE

Before conducting the baseline experiment with CH_4-air mixture, one set of experiment was performed with air (cold flow) only. Figure 4.3 shows the non-reacting flow field for air with a flow rate of 6 g/s. It shows that the swirler generates a gradually expanding flow area towards downstream with the lower area next to the swirler tip. The high velocity flow zones reside close to the combustor walls providing enough space for recirculation of flow between them. The swirler also generates vortices which propagate downstream through the recirculation zones. Thus, the presence of two high velocity flow regions near the combustion chamber walls with strong recirculation zones between them helps stabilizing the flame right in front of the swirler tip during combustion.

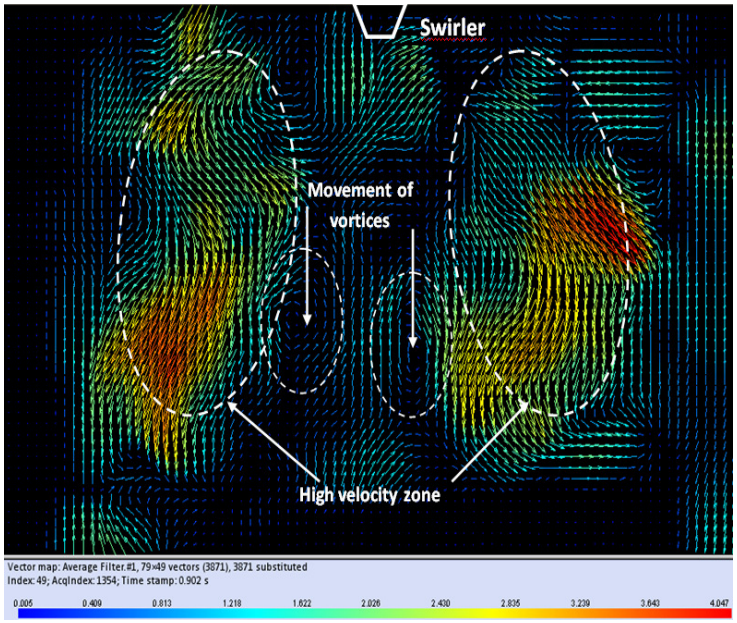

Figure 4.3 Non-reacting flow field for air flow with a flow rate of 6 g/s.

The flashback limits for combustion of Methane in the swirl stabilized combustor are shown in Figure 4.4. It demonstrates that Methane has the tendency to increase its flashback propensity with increasing air flow rate up to a certain value (approximately 3 g/s for the present combustor). After this, the flashback propensity keeps decreasing even the air flow rate is increased. The changes in the CH_4-air flame flow field during a typical flashback event is shown in Figure 4.5. It can be seen in Figure 4.5 that, at relatively lower equivalence ratio the high-velocity flame stabilizes close to the combustion chamber walls allowing the low-velocity recirculation zones to form between them. With the increase of equivalence ratio, the balance between the recirculation tip and the flame tip is disturbed; this causes the volume of the recirculation zones to reduce, see frame (b). When the equivalence ratio crosses the critical value, the flame goes back to upstream distorting the recirculation zones. The complete distortion of the recirculation zones is seen frame (c), which represents the flashback condition.

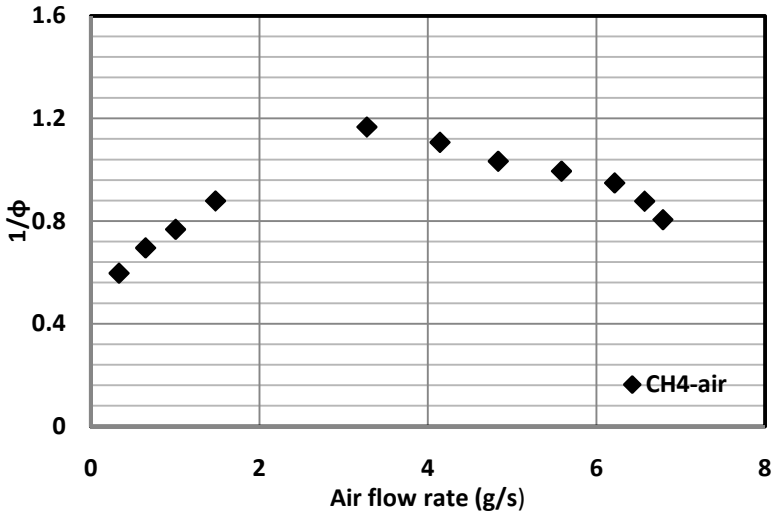

Figure 4.4 Flashback limits for Methane-air flame in the swirl stabilized combustor.

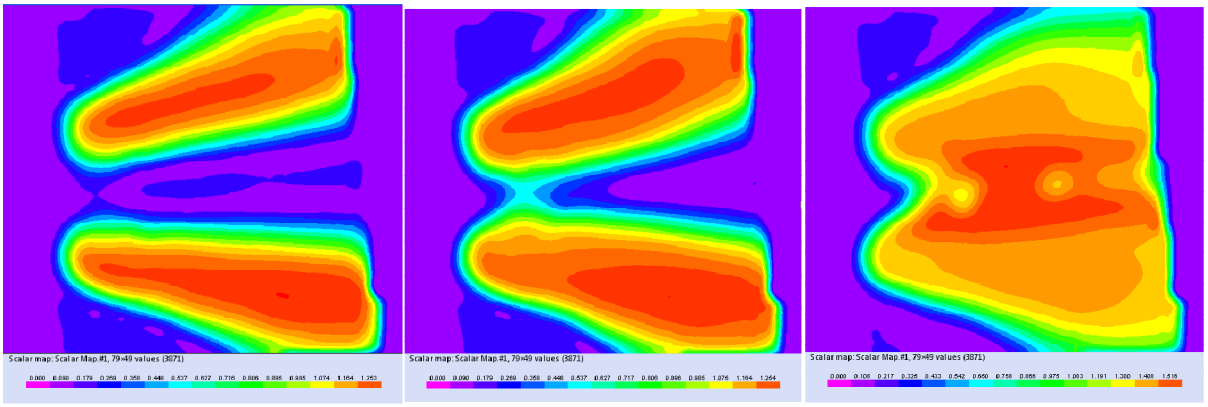

(a) (b) (c)

Figure 4.5 Change in the reacting flow field during a typical CIVB flashback phenomenon for CH_4-air mixture

4.3 EFFECT OF FUEL CONCENTRATION IN H_2-CO MIXTURE

Figure 4.6 shows the flashback limits for different H_2-CO compositions. A comparison of the flashback limits of these fuel compositions with those of Methane is also presented in this plot. Since H_2 possesses much higher burning velocity than Methane, H_2-CO fuel mixture undergoes CIVB flashback at leaner condition than Methane. The effect of H_2 concentration in different H_2-CO mixture compositions on the CIVB flashback is also clearly evident in the plot. For a given air mass flow rate, the equivalence ratio at which CIVB flashback occurs decreases with an increase of H_2 concentration in H_2-CO fuel mixtures, i.e. the presence of high percentage H_2 in the mixtures tends to shift the operating

conditions of the combustor into flashback regime. The increase of H_2 percentage changes the kinetics and the thermophysical characteristics of the mixture that accelerates the flame propagation.

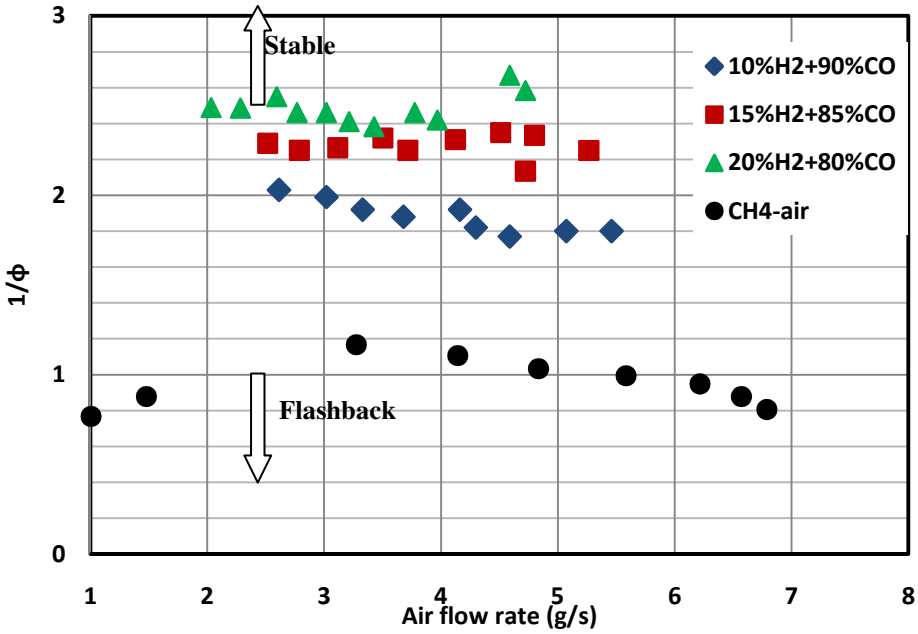

Figure 4.6 Comparison of the flashback limits of various H_2-CO mixture compositions with that of CH_4-air mixture.

The flow visualization images shown in Figure 4.7 show how the flow field shifts from a stable state to a CIVB driven flashback condition for 10%H_2 + 90%CO mixtures. Figure 4.8 represents the same process but with 20% of H_2 in the fuel mixture. In both the figures, frame (a) represents the stable flame situation and frame (f) represents the flame underwent CIVB flashback. As seen on figures 4.7 and 4.8, flames are initially stabilized on the tip of the centerbody forming recirculation zones in the middle of the two high-velocity flame locations. Vortices V_1, V_2 and W_1, W_2 are seen to propagate through the recirculation zones on the left and right sides, respectively. Due to higher percentage of H_2 in the fuel mixture, much extended stable flames are observed to generate at lower equivalence ratios in Figure 4.8. On the other hand, the stable flames at lower equivalence ratios in Figure 4.7 are relatively shorter and thinner; this causes the formation of relatively spacious recirculation zones when compared to those in Figure 4.8. As a result, the propagation of vortices through the recirculation zones is more prominent in Figure 4.7. With the increase of equivalence ratio, the cross-sectional areas of the recirculation zones become narrow, see frame (d). Once the equivalence ratio exceeds a critical value,

the flame goes back to upstream distorting the recirculation zones. The complete flame flashback condition can be seen in frame (f).

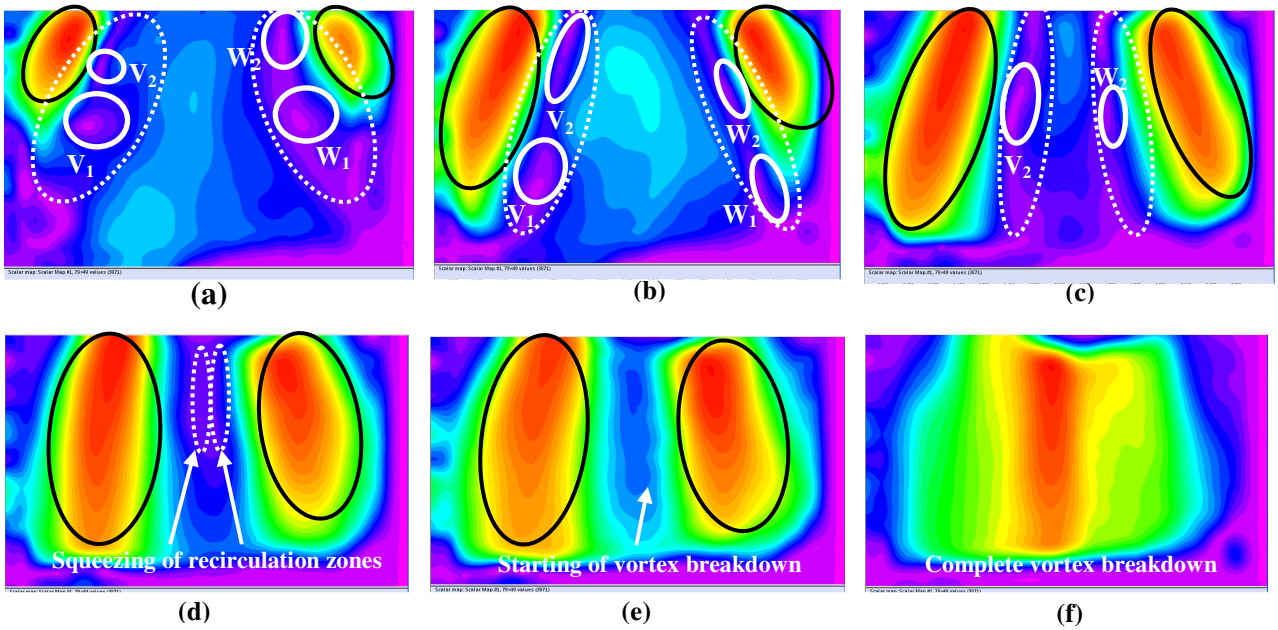

Figure 4.7 Sequence of a CIVB flashback for a fuel mixture of 10% H_2 and 90% CO; areas enclosed by solid black, dotted white, and solid white lines represent the approximate location of flames, recirculation zones, and vortices, respectively.

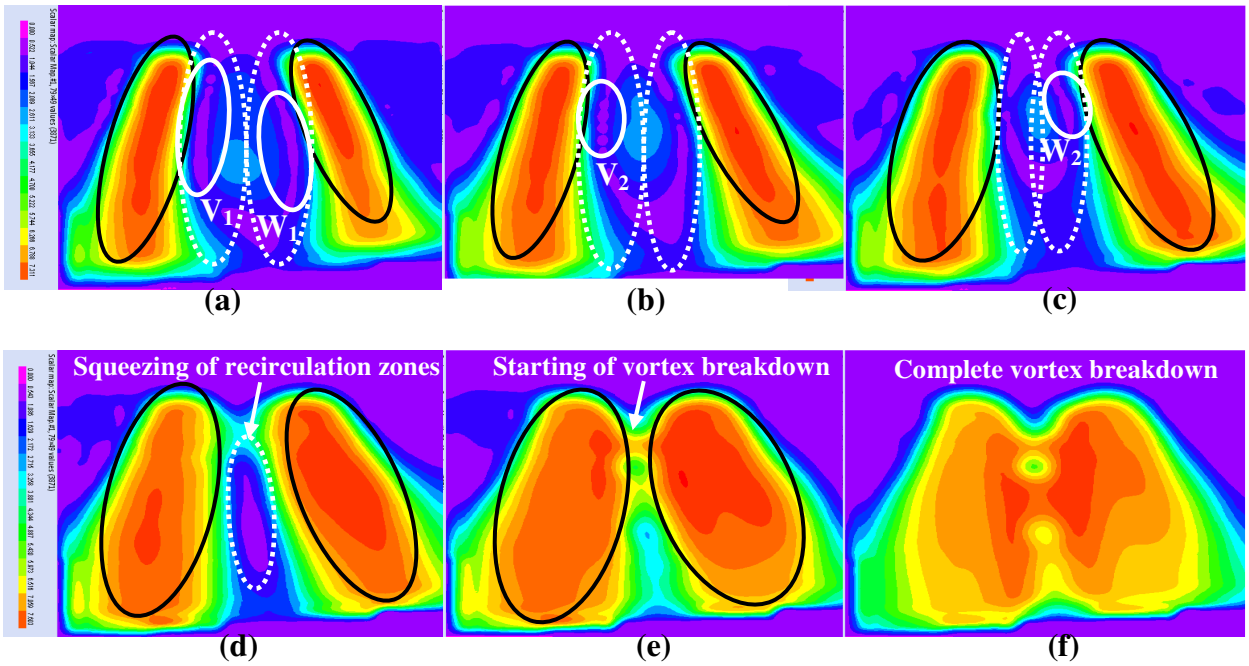

Figure 4.8 Sequence of a CIVB flashback for a fuel mixture of 20% H_2 and 80% CO; areas enclosed by solid black, dotted white, and solid white lines represent the approximate location of flames, recirculation zones, and vortices, respectively.

A comparison of frames (f) reveals that during flashback, 20%H_2+80%CO blend flame possesses higher backward velocity momentum compared to that of 10%H_2+90%CO blend flame. The percentage of H_2 dictates the intensity of flashback due to its high thermal and mass diffusivity. It creates complex vortex-chemistry interaction inside the recirculation zones; finally, breakdown the recirculation zones and pushes the flame upstream.

Figures 4.5, 4.7 and 4.8 present the flow visualization of a typical flashback sequence for CH_4 and H_2-CO fuel blends, respectively. A comparison of image 4.5(a) with images 4.7(a) and 4.8(a) reveals that H_2-CO-air flow field has little bit wider recirculation zones than those of CH_4-air flame flow field. The pressure gradient inside the flame due to hot gas expansion is more significant in the case of H_2-CO flame. However, it is evident from all there set of images that there is no significant difference in the flashback mechanism for CH_4 and H_2-CO fuel blends. In both cases, swirler generates stable flames close to two side-walls of the combustion chamber at low equivalence ratio allowing sufficient space for the formation of recirculation zones. As the equivalence ratio increases, the balance between the recirculation tip and flame tip is disturbed. At a critical equivalence ratio, the recirculation zones are broken down, causing the flames to propagate upstream.

4.4 EFFECT OF FUEL CONCENTRATION IN ACTUAL SYNGAS MIXTURES

H_2 and CO are the two major constituents of syngas fuels, although significant amount of N_2, CO_2, CH_4, and higher hydrocarbons are also present in the fuel mixture depending on the feedstock and gasification methods. To produce combinations of actual syngas fuels H_2, CO, N_2, CO_2, and CH_4 were mixed according to their percentages indicated in Table 4.1.

Table 4.1 Syngas composition from different coal sources

Gasification	Types of coal	CO (%)	H_2 (%)	CH_4 (%)	N_2 (%)	CO_2 (%)	Calorific Value (MJ/m^3)
Coal	Brown Coal	16	25	5	40	14	6.28
	Bituminous	17.2	24.8	4.1	42.7	11	6.13
	Lignite	22	12	1	55	10	4.13
	Coke	29	15	3	50	3	6.08

CIVB flashback limits measured for four different syngas compositions are shown in Figure 4.9. The flashback data plotted in this graph also indicates approximately the similar pattern to those observed by H_2-CO fuel blends. For a given air mass flow rate, flashback is primarily dominated by the percentage of H_2 in the blend; the higher the percentage of H_2 in the mixture, the more susceptibility to flashback. Therefore, brown coal and bituminous, containing higher percentage of H_2, are more inclined to flashback in comparison to lignite and coke for the same air mass flow rate.

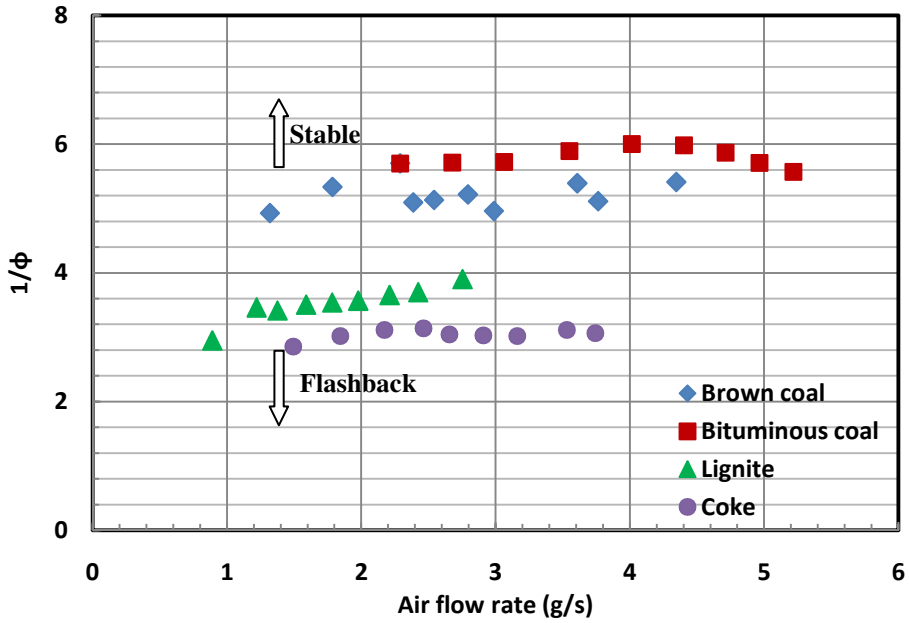

Figure 4.9 Flashback limits for actual syngas composition.

Again, two sets of flashback limits data are prominent in Figure 4.9. Brown coal and bituminous, lying on the higher air excess ratio side, contain approximately equal percentage of H_2. Hence, for a given air mass flow rate, their flashback limits are not too far from each other. Similarly, lignite and coke produced flashback limits data on the lower air excess ratio side which are closer to each other as they have comparable percentage of H_2.

The presence of CO in syngas fuels also plays a vital role on flashback limits. Although coke has higher percentage of H_2 than lignite, it is less prone to flashback in comparison to lignite. It is the higher percentage of CO in coke than lignite that plays the dominant role over the higher percentage of H_2 (in coke than lignite). The presence of CO in the fuel mixture produces termination reactions.

Of the two major diluents CO_2 and N_2, CO_2 has more dominance over N_2 on the flashback limits. Since brown coal and bituminous possesses almost similar quantities of H_2 and CO, their flashback limits are closer. However, still there exists a gap between their flashback data; this is due to the dominance of CO_2 over N_2. The higher percentage of CO_2 in brown coal retards its flashback propensity. Therefore, for a given air mass flow rate brown coal flame undergoes CIVB flashback at relatively rich condition in comparison to bituminous flame. CO_2 restricts the active free radicals, makes complex reaction, and finally increases recombination react

5. Numerical Results

The numerical models presented in this section where validated using the flow field data yielded by the experimental results described in chapter 4 for both isothermal and reacting conditions. The reacting simulations were performed using the Eddy Dissipation Concept (EDC) combustion model and Reynolds Averaged Navier-Stokes and LES for the turbulence model; the theory behind the models can be found in chapter 2.

5.1 COMPUTATIONAL DOMAIN

The domain used for the numerical simulations is identical to the experimental setup described in Chapter 3. A three dimensional model of the Gas Turbine Combustor was built in Unigraphics, and then the model was exported to Gambit as a parasolid (Figure 5.2). The grid was generated using Gambit. The final 3 dimensional mesh contained 800,000 elements.

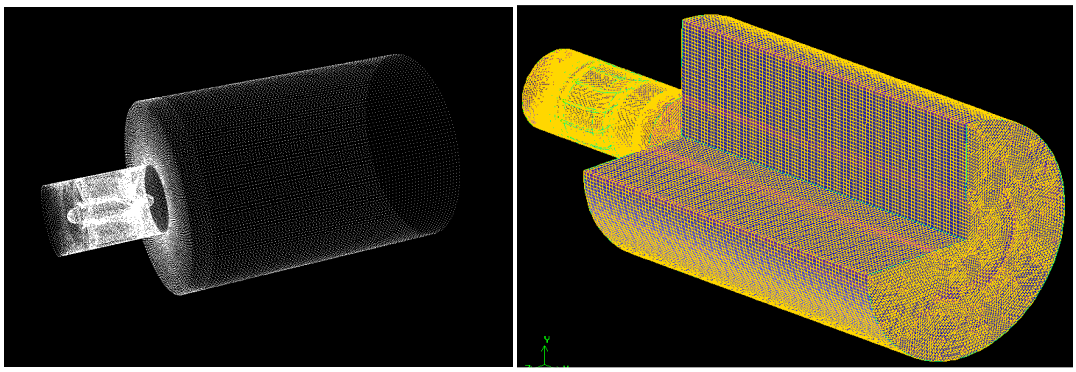

Figure 5.2 Grid used for the numerical computations

5.2 COLD FLOW

Simulations were run using two different modeling packages and then the results were compared with experimental data. For the validation of the models, an ensemble average of the flowfield yielded by the Particle Image Velocimetry (PIV) was used, see figures 5.3 and 5.4. For that run, the bulk velocity was 3.3 m/s; the same bulk velocity was chosen for the simulations run with both packages.

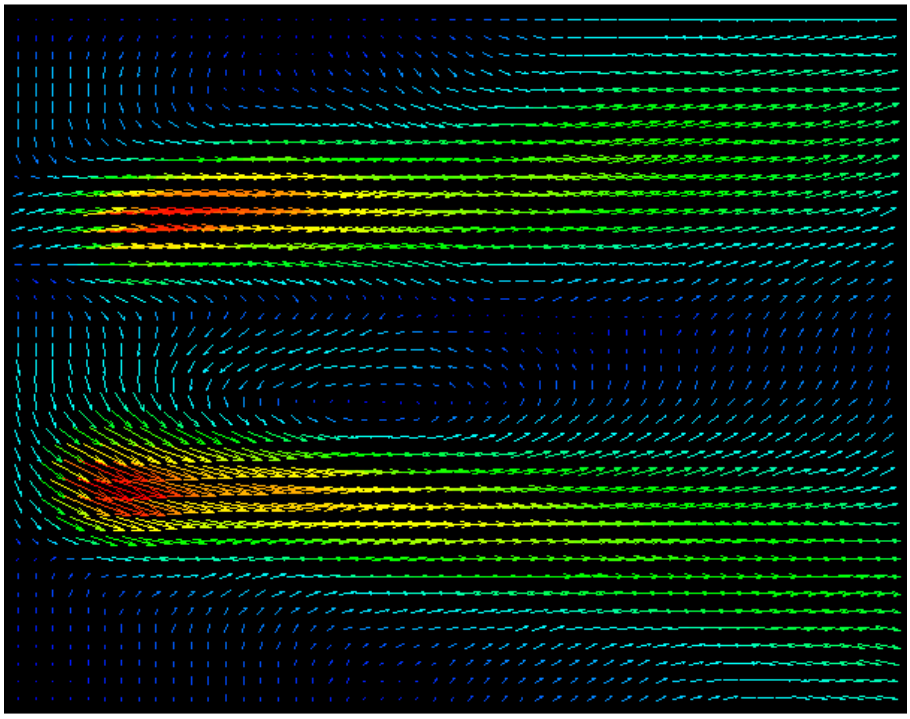

Figure 5.3 Ensemble average of 1500 frames of the flow filed of a cold flow run with a bulk velocity at the inlet of 3.3.

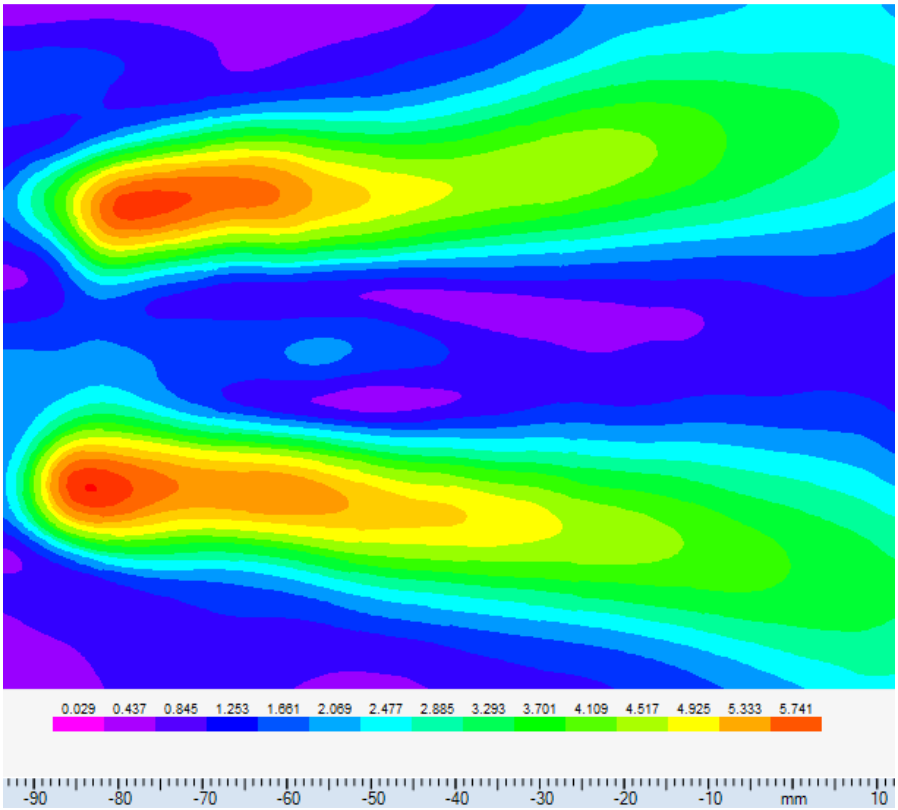

Figure 5.4 Ensemble average of 1500 frames of the scalar map of the velocity magnitude of a cold flow run with a bulk velocity at the inlet of 3.3

For validation purposes a Reynolds Average Navier-Stokes (RANS) turbulence model was chosen for both Fluent and OpenFOAM. Figure 5.5 compares the velocity field for Fluent and OpenFOAM for isothermal computations. The top part of the figures represents Fluent, and the bottom part represents OpenFOAM.

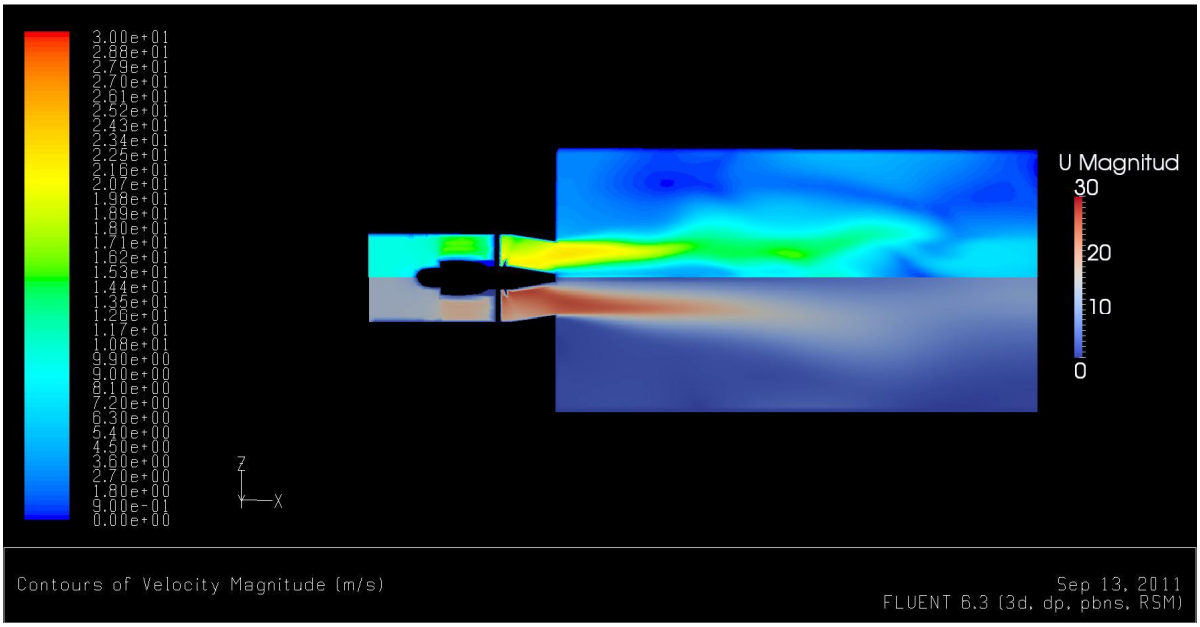

Figure 5.5 RANS simulation comparing the velocity field for Fluent (top) and OpenFOAM (bottom)

The velocity profiles of the velocity component in the axial direction were compared for the experimental data and both models. Figures 5.6, 5.7, 5.8 and 5.9 show the velocity profile of the ensemble average of the experiments and RANS computations for Fluent and OpenFOAM at 2 cm from the nozzle exit, at 5 cm, at 6 cm and at 10 cm respectively.

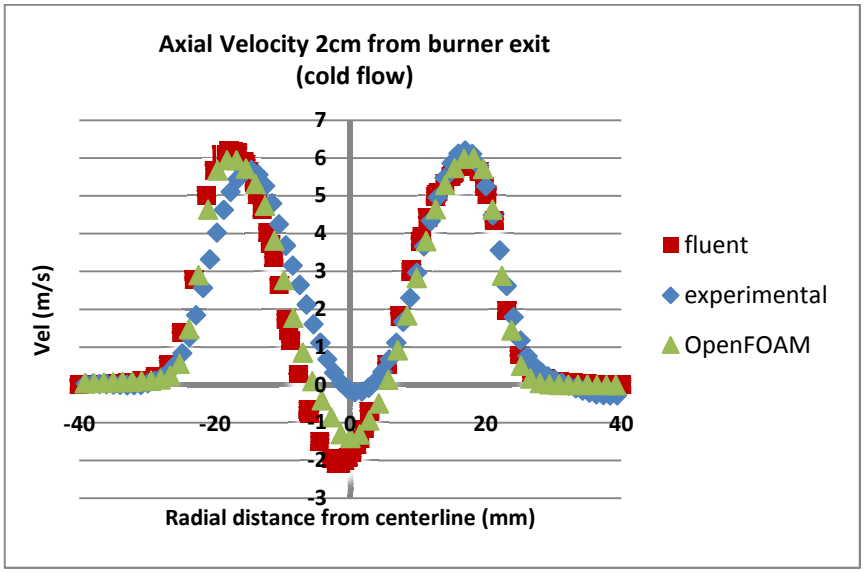

Figure 5.6 Axial velocity comparison at 2cm from the burner exit

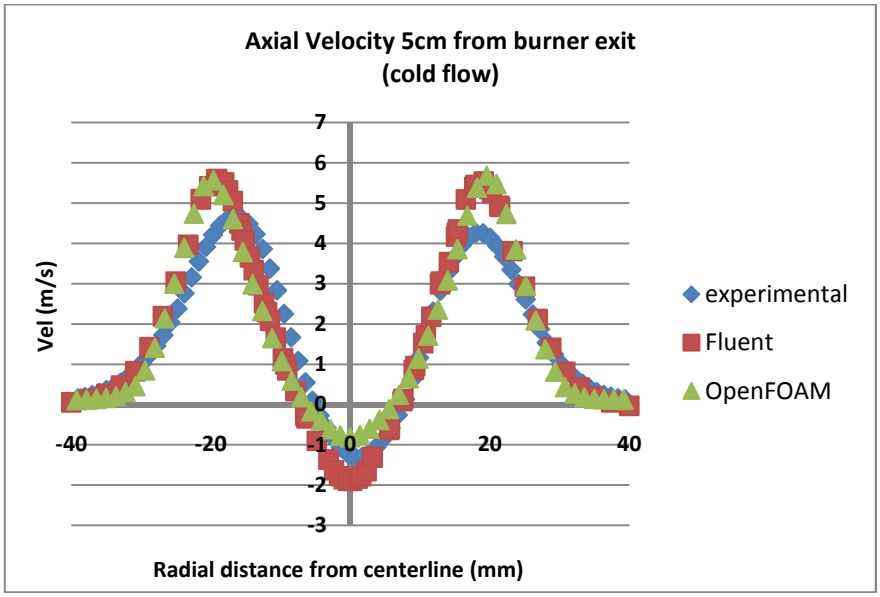

Figure 5.7 Axial velocity comparison at 5cm from the burner exit

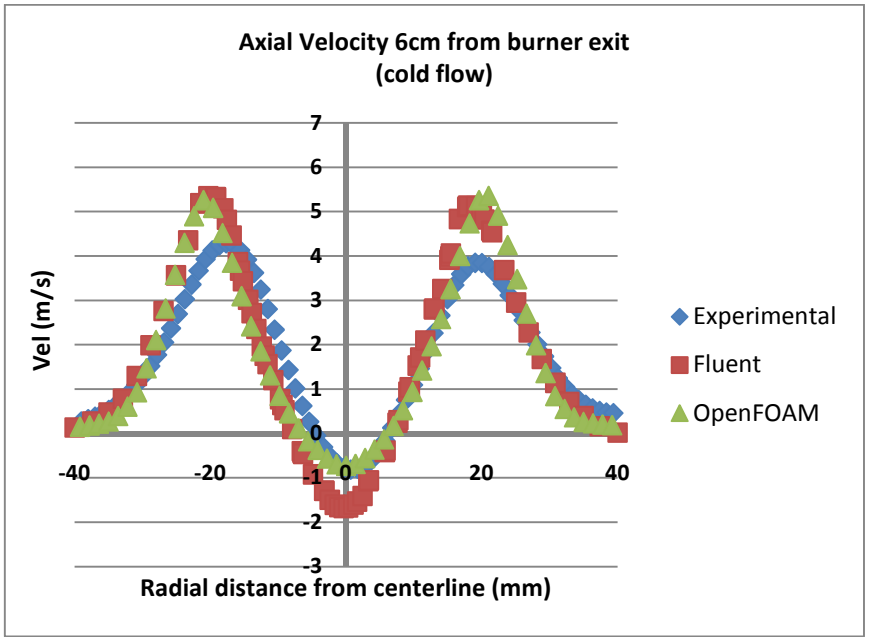

Figure 5.8 Axial velocity comparison at 6cm from the burner exit

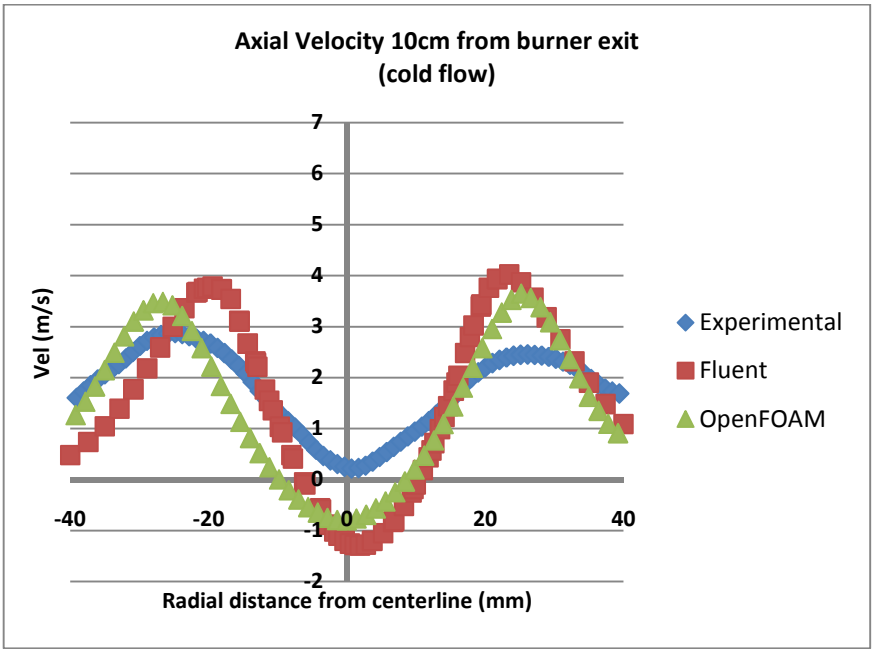

Figure 5.9 Axial velocity comparison at 10 cm from the burner exit

It can be observed from the velocity profiles that there is a very good correlation between the results from Fluent, OpenFOAM, and the experiments. There is a better correlation closer to the burner exit than further downstream. It can also be observed that the models are over predicting the strength of the recirculation zone.

5.3 REACTING FLOW

A perfectly premixed mixture of methane-air with an equivalence ratio of 0.9 was injected into the combustion chamber initially held at ambient conditions (1 atm, 298K). The mixture was then ignited upstream of the swirler. The rection zone was then observed to propagate upstream and stabilize on the centerbody of the swirler. A RANS model for turbulence was chosen in order to make easier the comparison of the flowfield with the experimental data. An LES simulation was run next in order to investigate the transient phenomena that occurs in the combustor. It was found that the 3 dimensional vorticity field on the simulations helps explain the behavior of the flowfield on the actual experiments. The vorticity field is unsteady and therefore can only be accurately reproduced with the use of a model that accounts for time such as LES.

For the combustion model a species transport with eddy dissipation concept for treating the turbulence-chemistry interaction with detail chemical mechanisms was used. Because of the high computational demand of LES and the extra transport equations for the species, a reduced mechanism, consisting of 2 steps and 7 species was used.

5.3.1 Velocity field

RANS validation

Figure 5.10 shows a comparison of the flowfield for experiments and simulations for conditions described in the previous section. It can be seen from the picture that two high velocity zones develop after the mixture enters the combustion chamber and also a recirculation zone anchored to the certerbody of the swirler can be observed. Figure 5.10 helps to get an idea of the extent of the domain that the PIV covers in the chamber.

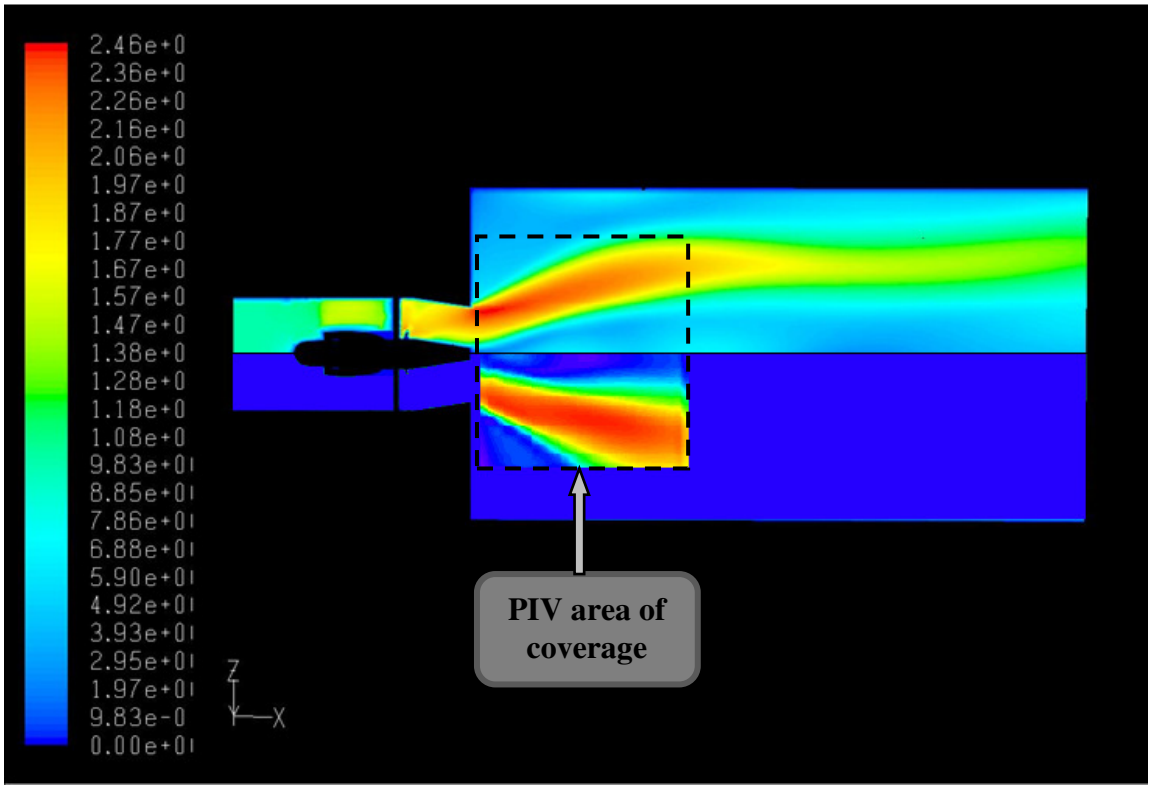

Figure 5.10 Flowfield comparison of experiments and computations. Top part of the image is a simulation, the bottom part are experimental results

Figures 5.11, 5.12, 5.13, and 5.14 show the velocity profile in the axial direction of the ensemble average of the experiments and RANS computations for Fluent at 2 cm from the nozzle exit, at 5 cm, at 6 cm and at 10 cm respectively.

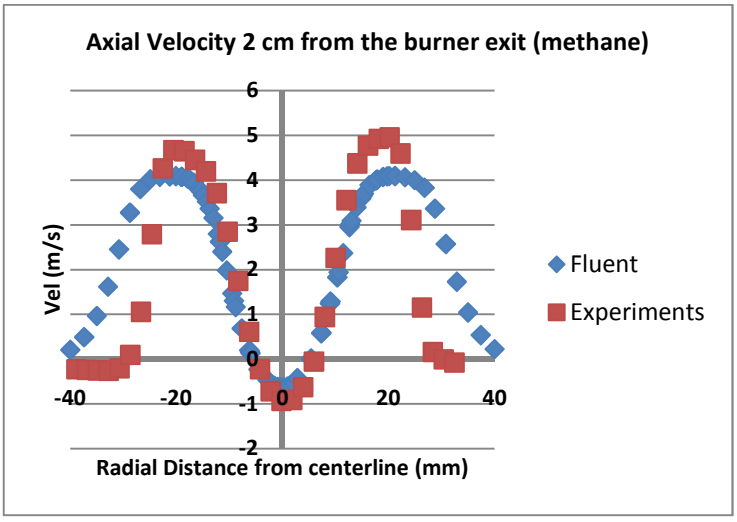

Figure 5.11 Axial velocity comparison of experiments and simulation at 2 cm from the burner exit

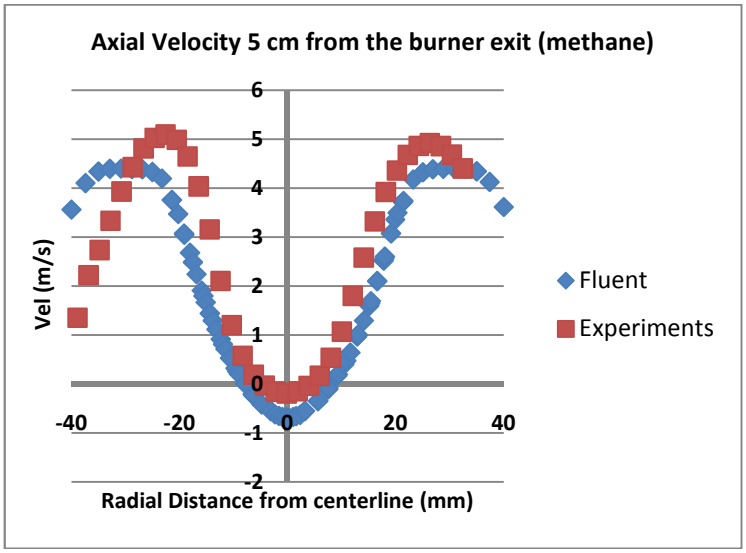

Figure 5.12 Axial velocity comparison of experiments and simulation at 5 cm from the burner exit

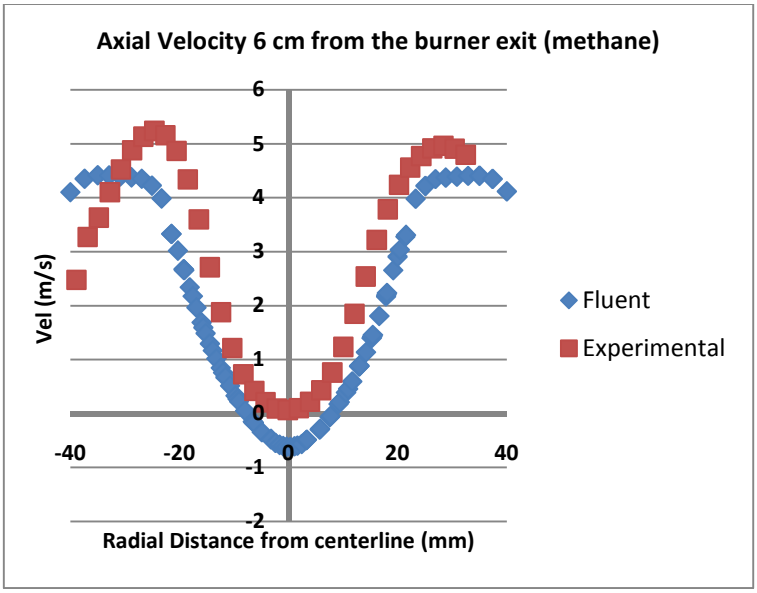

Figure 5.13 Axial velocity comparison of experiments and simulation at 6 cm from the burner exit

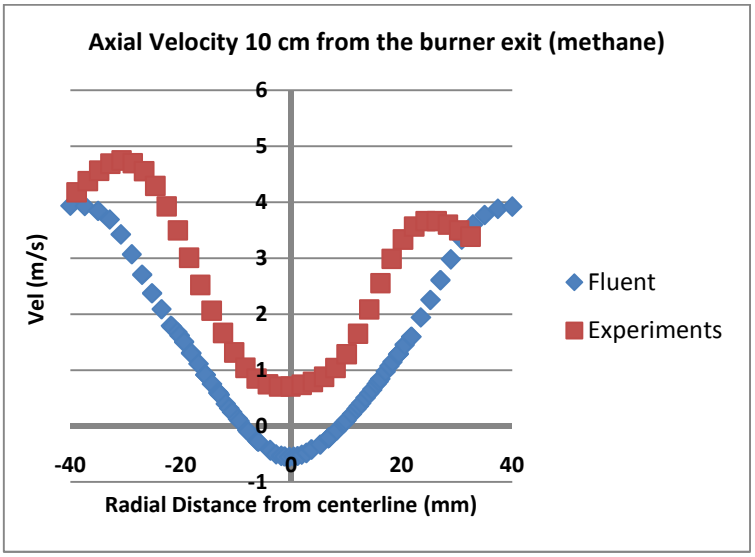

Figure 5.14 Axial velocity comparison of experiments and simulation at 10 cm from the burner exit

From the velocity plots it can be seen that there is a close correlation between the ensemble average of the experiments and the simulations. But in order to study the flowfield in detail instantaneous measurements and transient models for turbulence must be compared.

LES

The sequence shown in figure 5.15 depicts the evolution of the velocity field in the combustion chamber using LES. Figure 5.16 shows a sequence of the velocity field evolution for the same conditions for the experiments.

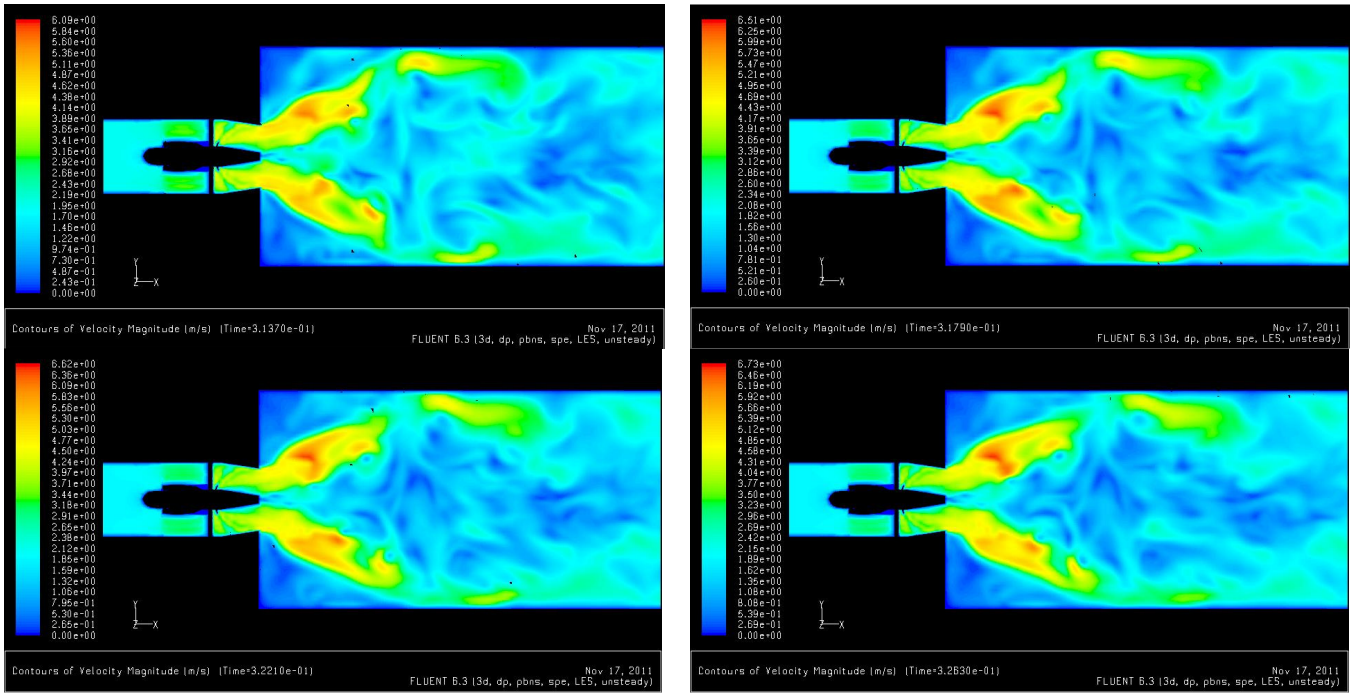

Figure 5.15 Flowfield sequence of LES simulations showing the evolution of the flow

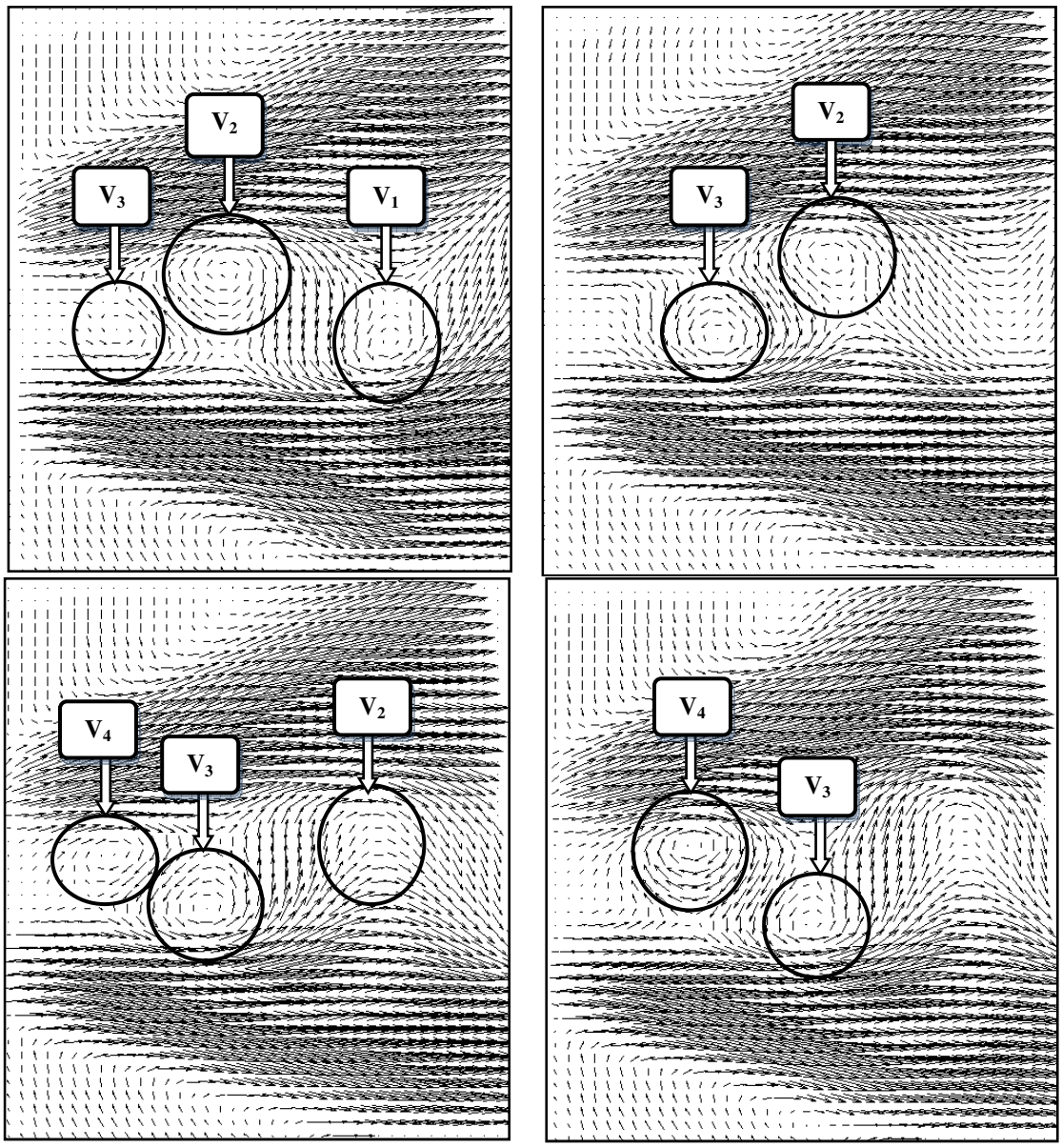

Figure 5.16 Flowfield sequence of experimental data showing the evolution of the flow

A very interesting pattern can be observed both on the experiments and on the simulation. Regarding the formation and downstream movement of the vortices; there is an alternation pattern were a vortex forms at the centerbody and moves downstream close to the high velocity zone, the next votex that forms will move downstream but this time attached to the other high velocity zone and this pattern repeats itself. Since these vortices are essentially "blobs" of vorticity, this behavior can be better appreciated using the vorticity field.

5.3.2 Vorticity field

Vorticity is basically the rotational spin of the fluid, and is defined mathematically as the curl of the velocity, $w = \nabla \times \boldsymbol{u}$. The sequence shown in figure 5.17 depicts the evolution of the vorticity field in the combustion chamber using LES. Figure 5.18 also shows a sequence for the vorticity field evolution for the experiments.

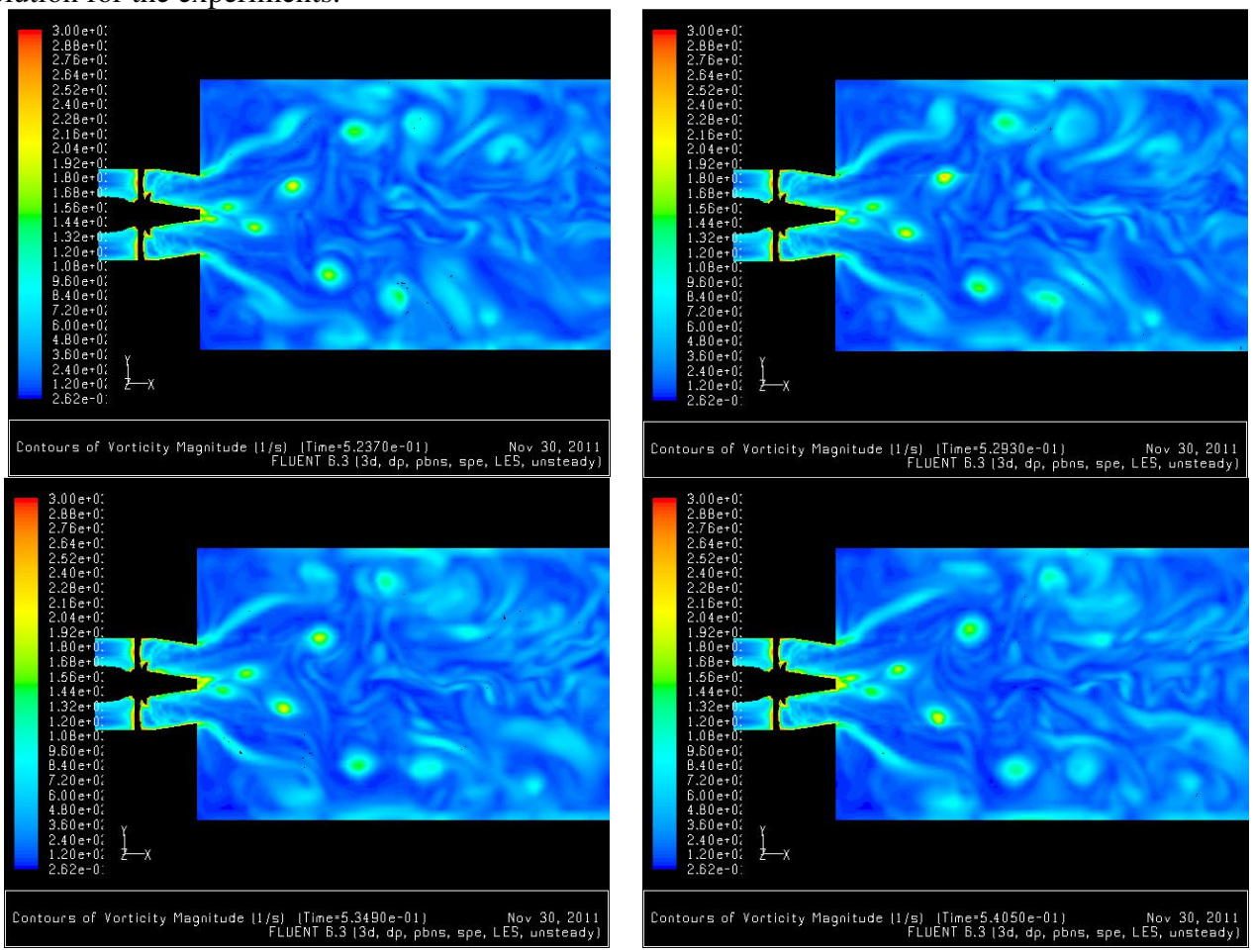

Figure 5.17 Sequence of LES simulations showing the evolution of the vorticity field

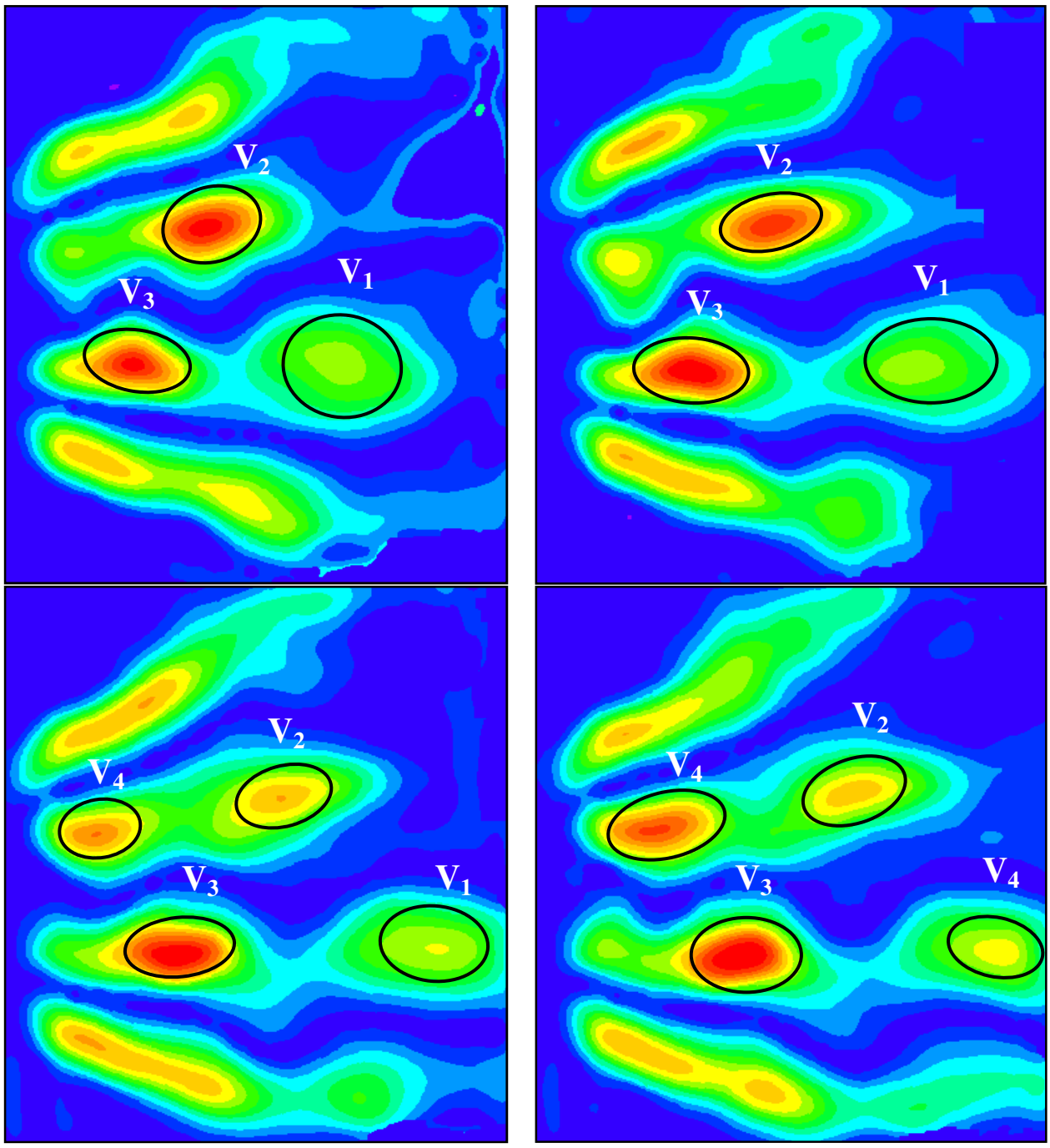

Figure 5.18 Sequence of experimental data showing the evolution of the vorticity field

Using the vorticity field in both experiments and simulations shows more clearly the pattern that develops on the velocity field. An advantage that simulations have over experiments is that we can extract data from the entire domain and not just a 2 dimensional plane. So if we see the three dimensional vorticity field shown in figure 5.19 we can appreciate better the nature of this phenomena.

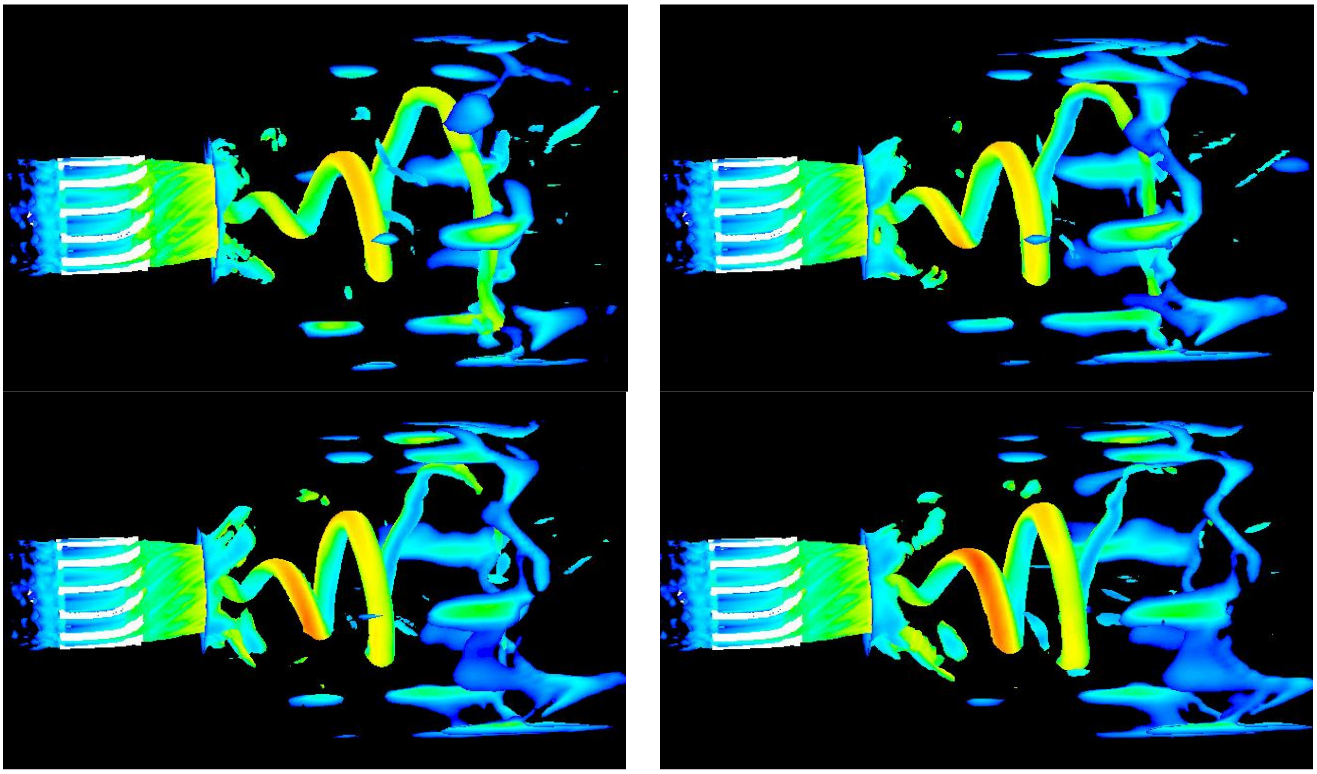

Figure 5.19 Three dimensional vorticity field evolution using of LES

It can be seen from figure 5.19 that there is a vortex spiral that originates at the centerbody and rotates periodically with respect to the centerline, this type of vortex breakdown has been previously studied by Lucca-Negro et. al. It is this vortex spiral the one that generates the votices observed on the velocity field on the experimental data. This can be more clearly observed in figure 5.20 where the three dimensional vorticity field has been super imposed on the two dimensional velocity field.

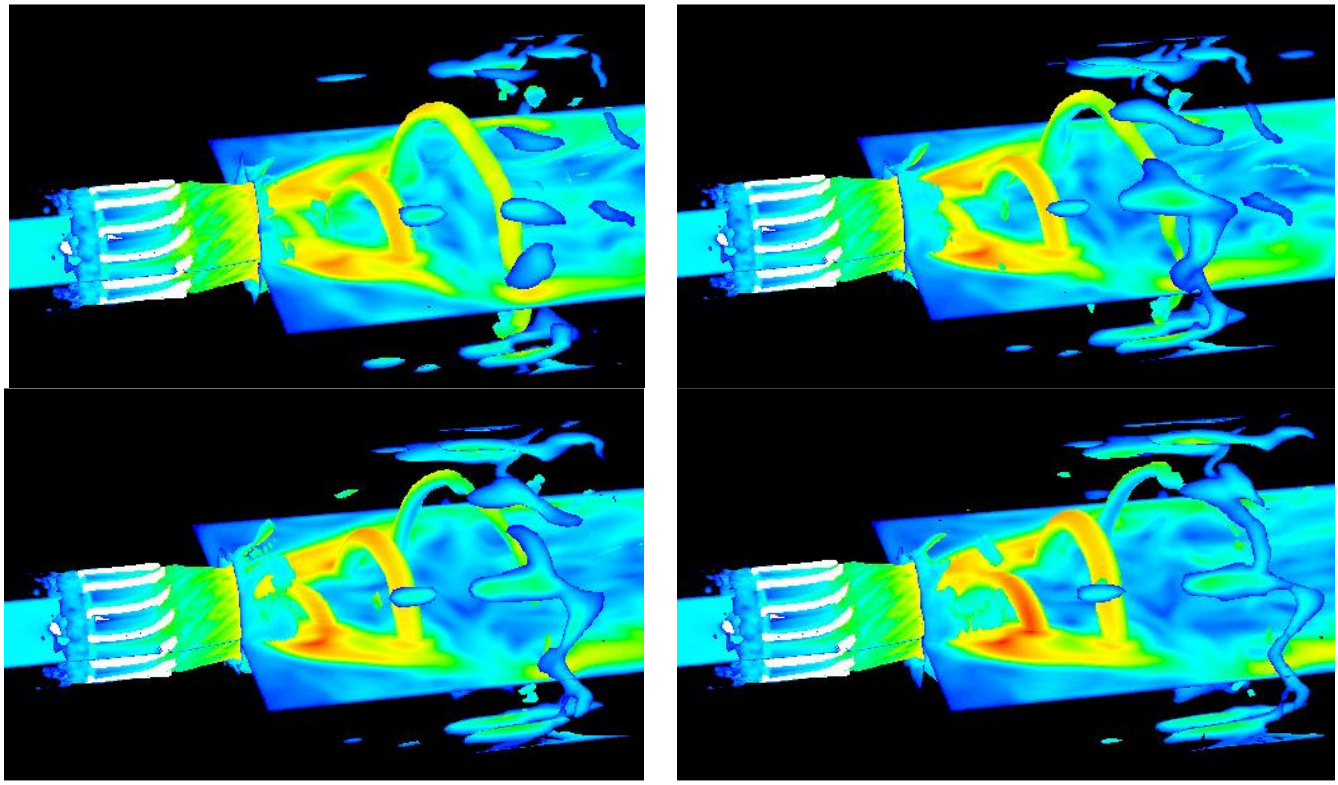

Figure 5.20 Three dimensional vorticity field with the 2 dimensional velocity field.

The sequence shown in figure 5.20 explains in a three dimensional fashion the behaviors observed in the velocity field that appear in the experimental data. The vorticity field is a very powerful tool to help describe and visualize the flowfield.

6. Conclusion and Future work

It is concluded in this study that when the hydrogen content of the fuel mixture is increased, for any given flow rate, the flashback propensity of the combustor increases. It was determined as well that syngas fuel derived from coals containing higher hydrogen content such as Brown and Bituminous are more prone to flashback than syngas derived from Lignite or Coke coal; this conclusion is congruent with the finding that hydrogen content increases the flashback propensity of a fuel mixture.

From the flow visualization experiments, it was observed that when the combustor is operating in a stable condition a bubble type recirculation zone is formed right after the centerbody. This recirculation zone ensures efficient combustion conditions by allowing good fluid mixing and offering long residence time for complete reactions to take place. However, when the operating conditions shift closer to the flashback regime the bubble type recirculation zone breaks down and transforms into a spiral type vortex, which is characterized by a rapid deceleration of the flow, followed by a corkscrew-shaped twisting of the flow [9]. The modeling effort in this study effectively reproduced this vortex breakdown phenomenon, helping visualize better the results yielded by the imaging system.

A high pressure combustor will be added to the experimental facilities of the cSETR shortly after this study is completed. Thorough experiments will be performed on the new combustor to test the operational limits (flashback and blowout) using different fuel compositions. Flow characterization will be performed using the high speed PIV system to determine the effects of the fuel composition and aerodynamic effects and the results will be compared with the combustor used in this study. The next step in the project would be to model the transition of the vorticity field from a bubble type recirculation zone to a spiral type and compare the simulations with the experimental results. This vorticity analysis would help visualize the changes in the flowfield leading to flashback.

References

[1] Peters, Norbert. *Turbulent Combustion*. Cambridge [England: Cambridge UP, 2000.

[2] Lieuwen, Timothy C., Vigor Yang, and Richard A. Yetter. *Synthesis Gas Combustion: Fundamentals and Applications*. Boca Raton: CRC, 2010.

[3] Pierce, Charles D. Progress Variable Approach for Large Eddie Simulation of Turbulent Combustion. Diss. Stanford University, 2001.

[4] Wang, Ping. Large Eddy Simulation of Turbulent Swirling Flows and Turbulent Premixed Combustion. Diss. Lund Institute of Technology, 2005.

[5] De Villiers, Eugene. The Potential of Large Eddy Simulation for the Modeling of Wall Bounded Flows. Diss. Imperial College of Science, Technology and Medicine, 2006.

[6] *Annual Energy Outlook 2011*. Rep. no. 0383. US Energy Information Administration

[7] "Clean Energy, US EPA." *US Environmental Protection Agency*. Web. 01 Dec. 2011. <http://www.epa.gov/cleanenergy/energy-and-you/affect/air-emissions.html>

[8] Gupta, A. K., Lilley, D. G., and Syred, N. (1985), Swirl Flows, Abacus Press, Cambridge, Massachusetts, USA.

[9] Lucca-Negro, O., and T. O'Doherty. "Vortex Breakdown: a Review." *Progress in Energy and Combustion Science* 27 (2001): 431-81.

[10] Dam, B., Corona, G., Love, N., and Choudhuri, A., 2010 “Investigation of Flashback Propensity in Turbines with Syngas Fuels”, *Journal of Fuel*, submitted for review.

[11] Kroner, M., Fritz., J., and Sattelmayer, T. (2001), “Flashback in a Swirl Burner with Cylindrical Premixing Zone,” ASME Paper No. 2001-GT-0054.

[12] Kroner, M., Fritz., J., and Sattelmayer, T. (2003), “Flashback Limits for Combustion Induced Vortex Brakdown in a Swirl Burner,” Journal of Engineering Gas Turbines and Power, Vol. 125, pp. 693-700.

[13] F. Kiesewetter, M. Konle, and Sattelmayer, T. (2007), “Analysis of Combustion Induced Vortex Breakdown Driven Flame Flashback in a Premix Burner With Cylindrical Mixing Zone” Journal of Engineering Gas Turbines and Power, Vol. 125, pp. 693-700.

[14] Tangermann, E. , Pfitzner, M. , Konle, M. and Sattelmayer, T.(2010) “Large-Eddy Simulation and Experimental Observation of Combustion-Induced Vortex Breakdown”, *Combustion Science and Technology*, Vol. 182, No. 4, pp. 505-516

[15] Kuo, Kenneth K. *Principles of Combustion*. Hoboken, NJ: John Wiley, 2005.

[16] Swaminathan, Nedunchezhian, and K. N. C. Bray. *Turbulent Premixed Flames*. Cambridge: Cambridge UP, 2011.

[17] M. Chapuis, C. Fureby, E. Fedina, N. Alin & J. Tegnér “LES Modeling of Combustion Applications Using OpenFOAM”, *V European Conference on Computational Fluid Dynamics,* ECCOMAS CFD 2010, Lisbon, Portugal, 14-17 June 2010

[18] G. Tabor and H.G. Weller, “Large Eddy Simulation of Premixed Turbulent Combustion Using Xi Flame Surface Wrinkling Model”, *Flow, Turbulence and Combustion,* Vol. 72, No. 1, 2004, pp. 1-28

[19] Weller, H. G., G. Tabor, and A. D. Gosman. "Application of a Flame-wrinkling LES Combustion Model to a Turbulent Mixing Layer." *International Symposium on Combustion,* Vol. 27, No. 1, 1998, pp. 899-907.

[20] Davidson, P. A. *Turbulence: an Introduction for Scientists and Engineers*. Oxford, UK: Oxford UP, 2004.

[21] Pope, S. B. *Turbulent Flows*. Cambridge: Cambridge UP, 2000.

[22] Durbin, Paul A., and B. A. Pettersson. Reif. *Statistical Theory and Modeling for Turbulent Flows*. Chichester, West Sussex: Wiley, 2011.

Vita

Gilberto Corona was born in Chihuahua, Mexico in January 1987. The first son of Francisco Corona and Patricia Gallegos, he graduated from ITESM High School campus Chihuahua, in the spring of 2005 and entered The University of Texas at El Paso in the fall. While pursuing a bachelor's degree in Mechanical Engineering, he worked as an undergraduate research assistant for the Center of Space Exploration and Technology Research cSETR (Former Combustion and Propulsion Lab). He graduated from his bachelor's in Mechanical Engineering in the Fall of 2009 with high honors – Lambda Cum Laude. He entered the Graduate School at The University of Texas at El Paso in pursuit of a Master's degree in Mechanical Engineering working at the cSETR. Gilberto has presented his research findings in the area of Combustion and Gas Turbines in multiple international conferences and journals.

Permanent address: 4141 Westcity ct. apt 114
El Paso, Texas, 79902

This thesis/dissertation was typed by Gilberto Corona.